

Response to review comments of manuscript " Distinguishing between old and modern permafrost sources with compound-specific $\delta^2\text{H}$ analysis"

The Cryosphere Discussions doi:10.5194/tc-2017-17

We thank the three reviewers for their comments, and provide answers to these comments and suggestions below.

Black: review comment

Blue, italic: our response and edits in manuscript

Reviewer Trevor Porter

General comments:

Title should indicate the study region (e.g., Laptev Sea catchment, NE Siberia).

We have added "in the Northeast Siberian land-shelf system".

Abstract is one of the longest I've read in recent years. It includes a lot of useful information, but could (and probably should) be more concisely written. I leave this to authors and editor to decide.

We have shortened the abstract, as indeed it was rather long.

There is now a large body of literature on the isotopic composition of relict ice from ICD's in this very same region (see Opel et al. 2017 Climate of the Past; and references therein). These studies find that precipitation isotope composition recorded in these ICD's was highly variable during Pleistocene cold stages; for example, texture and pore ice 2H values range from roughly -250‰ to -160‰ between ca. 50-30 cal ka BP, while ice wedge values (winter precip) during the same interval range from roughly -260 to -230‰ . If the fossil plants were using the same water that is preserved in the pore ice, then there may be a significant amount of variance not yet captured in the n-alkyl dataset from the ($n = 9$) ICDs sampled in this study. The spatial distributions of distinct ICD units in this region are not equal (see Opel et al., 2017) and, thus, have different potentials for erosion and contribution to the blend of n-alkyls deposited on the shelf. I would like the authors to acknowledge this potentially major source of uncertainty. I would also ask the authors disclose any information they have on the age of the sampled ICDs and, if possible, cross-reference to the regional stratigraphy scheme outlined in Opel et al. (2017).

Thank you for highlighting this point. We had not seen the article by Opel et al. While it is still not a peer-reviewed published paper (status listed as "in discussion"), it clearly provides additional insight to ICD from this region. We have now cited this paper, as well as a few others in the Introduction (and elsewhere) of our revised paper. We agree that the point brought up can be a source of uncertainty, and have acknowledged this fact in section 4.2 quite extensively.

We have also added the ^{14}C information we have available on a few of the samples analyzed (Table 1). The new text reads as follows (line 492-510):

"Finally, we realize that the amount of soil and ICD samples analyzed in this study is limited, and want to point out that the results may change when more data are analyzed in the near future. Additionally, studies have shown that the $d^2\text{H}$ signature of ice within ICD permafrost deposits can range from roughly -150‰ to -260‰ depending on the type of ice (wedge ice vs. texture ice) as well as the period of formation (different Pleistocene cold stages) (Opel et al., 2017 and references therein). The source of water (i.e. type of ice) and age of the deposit will therefore influence the n-alkane or n-alkanoic acid $d^2\text{H}$ signal. However, regardless of the natural variability associated with the processes mentioned above, both ICD and texture-ice isotopic compositions appear to reflect long-term climate changes (Opel et al., 2017; Schwamborn et al., 2006; Dereviagin et al., 2013; Porter et al., 2016) which, likely, were also captured in the n-alkane or n-alkanoic acid $d^2\text{H}$ signal. Unfortunately, we do not have ^{14}C -ages available for all ICD samples, so cross-referencing to published stratigraphies in the region is not possible. Coastal sediments, however, will represent a

mixture of material released from different depths, outcrops, and stratigraphies within the catchment or coast. For source-apportionment applications, we reason that a growing body of leaf wax d^2H end-member data from the ICD region can overcome the variability issues highlighted above."

This paper would benefit from another figure that provides photographic examples of the ICDs and topsoil sections.

We do not have high-quality photographic material available from all the sites, unfortunately, but have added a figure as supplementary information with some examples.

Specific comments:

L44, The n-alkane sum and interquartile range given (210 ± 350 ug/gOC) implies negative concentrations are possible, and is not consistent with Figure 2a. This also occurs on L299. *Since we shortened the abstract, we have removed the n-alkane concentrations from the abstract (L44) but have changed the notation in (the previous) L299 as this was perhaps confusing. The interquartile range was 350 (Q1-Q3), so we have chosen to now report this as 210_{148}^{494} to make it more clear that IQR1 is 148 and IQR3 is 494. (lines 344-349 and lines 364-369). We have also adjusted Table 4.*

L149, instead of citing the IAEA website, better to cite a peer-reviewed article that supports your statement. Dansgaard (1964, Tellus) is appropriate. *OK, good suggestion, we have done this (line 160).*

L158, it might be worth stating the underlying assumption, that colder air temperatures during the Pleistocene generally correlate with $2H$ -depleted precipitation; therefore, long-chain n-alkyl $2H$ during Pleistocene cold-stages should also be depleted compared to present. Also note that 'colder' and 'drier' could have opposing effects. All other factors equal (e.g., biochemical fractionation), a drier atmosphere during Pleistocene cold-stages could result in a larger leaf water enrichment and $2H$ n-alkyls (if RH is lower, despite lower air temps), which would lessen the overall offset between modern and Pleistocene n-alkyl $2H$.

Thanks, this is a good suggestion. We have edited this sentence to now read "Despite the plant fractionation associated with kinetic and plant physiology (Sachse et al., 2012), we hypothesize that δ^2H signatures of leaf wax n-alkanoic acids and n-alkanes are more depleted in OC from permafrost deposits formed during the colder Pleistocene (generally correlating with 2H -depleted precipitation), compared to more enriched values in OC from active layer or surface permafrost formed during the warmer Holocene. " (lines 178-183)

L199-201, if species information is available for the grasses and birch, please indicate.

Both samples were grass samples, but one of them was collected in the tundra, and one of them further south in a birch forest. We have clarified this (line 227-229). Unfortunately, we do not have species information available.

L308, the sphagnum index could also include C23 (see Bush and McInerney, 2013, GCA). For modern sphagnum samples I've collected in NW Canada (>65N), C23 is usually abundant (unpublished data). This suggestion isn't critical, but might be a more accurate metric for sphagnum vs. woody plants. *We are aware that either C23 or C25 can be abundant, but meant to illustrate the general differences (very small) between the two sample types. But, for comparison we have now replaced the $C25/(C25+C29)$ ratio with $C23/(C23+C29)$ in Figure 2 and added the C23 ratio to Table 4. Also, we have added a sentence to the text (line 357-360). Here, the average values for topsoil vs. ICD samples are further apart, yet still not statistically significant.*

L345, please delete 'it seems'. If there is uncertainty, this can be described in a more quantitative way.

We have deleted it (line 407).

L519-521, unclear if you are talking about potential overprinting of the fossil 2H in situ (e.g., with water in the frozen ICD), or following transport and deposition on the shelf. Please clarify. Also, give a citation that supports the statement that overprinting is enhanced in low pH environments.

We have clarified this by stating that the environmental water can be coming from various sources (e.g. in situ or during transport after thaw). Also, we have removed the statement on low pH environments as we could not support this with a proper reference, and it is less relevant to our study (lines 603-607).

Anonymous reviewer #1

If a positive decision is made I have no other detailed comments than the references need to be looked over. Some of them even lack publication year.

We have carefully read through the references list and edited/corrected where needed.

Anonymous reviewer #2

General comments:

I think the abstract is too long, and that it goes into too much specific detail. I think that it could and should be made more succinct.

We agree. This point was also brought up by Reviewer Trevor Porter. We have shortened the abstract.

The phrase "molecular-bulk upscaling challenge" is used without enough introduction/ definition. I understand what you mean by it, but I think that it would be better to explain what this is exactly in a bit more detail.

We have added a bit more specific description the first time we use this definition, in the introduction: " This $\delta^{13}\text{C}$ - $\Delta^{14}\text{C}$ dual-carbon isotope approach carries the strong advantage that it operates on the bulk OC level, thereby circumventing the "molecular-bulk upscaling challenge". This challenge relates to issues associated with upscaling from the molecular isotope level to the bulk level. These issues relate to the relative concentration (n-alkanes and n-alkanoic acids represent only a fraction of the total OC) but also to processes such as selective degradation, differences in physical association, or dispersion differences. " (lines 132-138).

A general comment about the structure of the discussion is the separation of the ^{13}C - ^{14}C data from the bulk geochemistry. Why are these measurements not included in this grouping? If you measure ^{13}C or ^{14}C on a bulk sample, isn't that "bulk geochemistry"?

You might be able to circumvent this issue just by renaming the bulk section to "bulk elemental geochemistry" or something like that.

We do not really follow the reviewer here. In the first section of the discussion we talk about %C, C/N values, as well as $d^{13}\text{C}$ on bulk samples. As such, we named this section " ... bulk geochemistry ... as it includes both elemental and isotopic measurements on bulk samples. The same is the case for the first section of the Results.

One thing that I think is also missing from the discussion is some mention of the possibility that the terrestrial sampling density may have missed some of the possible heterogeneity in permafrost chemistry. I realize that it's not easy to sample in this part of the world, but is there any reason to think that the results might look different if you had soil samples from 50 more sites? Why or why not? This would apply to the 2H data, as well as the other data.

This is a valid point. We have added the following text to the manuscript, at the end of section 4.2: "Finally, we realize that the amount of soil and ICD samples analyzed in this study is limited, and want to point out that the results may change when more data are analyzed in the near future." (line 492-494)

Regarding the second point/suggestion of this review comment, we think it would be too speculative to give more detail regarding the possible differences in results if more data were to be obtained.

Specific comments:

Line 78 – change “into” to “in”

Changed.

Line 99 – Personally, I’m not a fan of non-standard acronyms like this (ICD in this case). They require an elevated level of buy in from the reader, which I think takes away from the accessibility of the manuscript. That’s just my opinion, there’s plenty of precedent for this kind of thing of course.

We realize there are different opinions with respect to acronym usage, but prefer to continue using it as this shorter version is commonly used and it also improves readability.

Line 137 – At the introduction of the 2H discussion, it might help to frame the study better if you begin by saying that you propose the new tool, as well as evaluate the performance using a suite of other geochemical data including the aforementioned ^{13}C -radiocarbon method.

This is a good suggestion. We have now in the revised ms better introduced our tools in the introduction: " We will evaluate the performance of this complementary tool using additional geochemical data as well as the bulk $\delta^{13}\text{C}$ - $\Delta^{14}\text{C}$ mixing approach." (lines 148-150).

Line 142-143 - These are nice papers, but they aren’t really the best references to support the assertion that “the isotopic value of local precipitation is a function of local climate”

Yes, we agree. We have added: Craig H. 1961. Isotopic variations in meteoric waters. Science 133: 1702–1703. (line 154)

Line 149 - If you mean to give the maximum range you could point out that precip in east africa can be upwards of +50 per mil, while the SLAP2 (Standard Light Antarctic Precipitation 2) standard is - 427.5 per mil.

We have edited this to now present the maximum range, using the values/locations that this reviewer provides (lines 160-163).

Line 162-168 – The end of the introduction falls a little flat in my opinion. At the moment you say what you do in your study, followed by a general statement about why it’s important to study these types of questions. What’s missing to me is a statement that directly comments on how what you do with this study will help with these important questions. As it is currently written it doesn’t setup the next section so effectively.

We see the point, and have therefore now added one more sentence that specifically mentions the use of our proposed tool, at the very end of the introduction: "Our proposed tool may be used to trace these temporal and spatial differences in OC release from permafrost thaw, as well as the extent of burial of OC in sedimentary reservoirs."(lines 191-193).

Line 195 - I think it is better to replace your internal lab sample codes with something more straightforward when reporting the results (things like “CH DY-3A” are meaningless to the reader and hard to remember). Include them in a data file or something if you want to be able to cross-reference with Vonk et al., 2013, but for presentation purposes I would simplify.

We have renamed the samples with TS-1, TS-2, ICD-1, ICD-2 etc, and include the original sampling ID in Table 1.

Line 232 – Remember to define acronyms at first use.
This acronym was defined in the previous paragraph.

Line 243 – Check super/subscripting for H₃⁺.
We have edited this into H₃⁺ (line 276).

Line 244 – Give units for H₃⁺.
We have added units (% per V) and have also added a reference for the use of H₃⁺ (Sessions et al., 2011) (line 277).

Line 248 - The “methylation effect” language is odd to me, since it makes it sound like what was quantified was the difference in 2H values between the derivatized and non derivatized standard, rather than the 2H value of the hydrogen in the added methyl group. Since the magnitude of the “methylation effect” will be different depending on what the 2H value of the covalently bonded hydrogen in the methylated fatty acid is in addition to the chain length, you want to do the correction by mass balance. Probably that is what you did, but the language doesn’t make it sound that way.

We agree, we have changed this into "methylation correction" (lines 281-282).

Line 251 – This call to table 5 is out of order since you haven’t called tables 2-4 yet.
This sentence is a general remark on how we report the d₂H values, so we decided to not call table 5 at this particular place.

Line 259 – Not sure what you mean exactly by “with mean and standard deviations obtained from the literature values”.
This was meant to refer to the end-member values for the d₁₃C-D₁₄C source apportionment, but is perhaps confusing. We have now specified this to "with mean and standard deviations obtained from our analysis (d₂H on TS and ICD samples) and from literature (13C and 14C on end-members)" (lines 298-299).

Line 296 – I might add a few words to the start of the sentence that begins on this line to make it clear that you are discussing distributions within individual samples, and that you are still talking about topsoil samples only.
We have done this by adding " for Topsoil-PF samples" to this sentence (line 343).

Line 318 – This call to table 3 is out of order.
Indeed, this should be table 2. In the previous sentence, however, we have changed a call to table 2 into table 3. As all tables have already been called before, we did not change the order of the tables.

Line 354 – spell check.
Thanks, we have corrected this.

Line 417 – change “proxies” to “proxy”
We have changed this.

Line 452 – This is the first mention of results from the shelf-slope samples. In the methods you point out a reference for more information on the sampling procedures, but what about the laboratory analyses and results? This should be included in the earlier sections.
Yes, good point. We have added a brief paragraph at the end of section 2.2 (lines 286-290).

Line 454 - I like how you use the individual n-alkanes rather than arbitrarily averaging them together.
Thanks.

Lines 481 – 500 – Somewhere in this section, or somewhere else in the manuscript if it fits better, it would be good to discuss how variability within an end member might impact the results. This is important for both the 2H and the 13C-radiocarbon approaches, but it seems like it would be especially important for the radiocarbon. In addition to the acknowledged aging along the transect won't there be different ages within a topsoil permafrost? How might this impact the results if melting/erosion occurs at different depths/ages within a site?

We agree that variability within the end-members plays an important role and should be taken into account. For the 13C and 14C approaches, the amount of end-member data available is fairly good (and growing) with 30-40 data points for 13C and >300 data points for 14C. This is described in the second paragraph of section 4.3. Our Markov Chain Monte Carlo mass-balance model actually accounts for the end-member variability (described and referenced in section 3.2). When thawing and erosion occurs at different depths or ages, at various locations throughout a watershed or coastline, the signal will be averaged when measured in coastal sediments. We have now acknowledged this important point (lines 505-507) (reviewer Trevor Porter also posted a related comment). Regarding the amount of d2H end-member data available: we are aware that our sample set only exists of n=9 data points for each source. Variability in the mean end-member values may therefore change (or, perhaps, decrease) when more data become available. We have now also briefly mentioned this point at the end of section 4.2 (lines 492-494).

Line 568 – As with the end of the introduction, I think that the end of the conclusion could go a little further to bring this study back together with the big picture goals. Remind us how “increasing our understanding of the fate of thawing permafrost in the coastal environment” will help us and why we should care about it.

We have added a bit more "big picture" text to place the results of our study into context with the general goals outlined in the introduction. The final paragraph of the conclusions now reads: "This study shows that $\delta^2\text{H}$ of leaf wax molecules has the potential to be used in quantitative source-apportionment studies of thawing permafrost in coastal or marine settings. It can serve as an alternative or complementary approach to the commonly applied bulk $\delta^{13}\text{C}$ - $\Delta^{14}\text{C}$ method. We recommend continuing data collection and optimization of end-member definition and calibration. Refining the molecular $d^2\text{H}$ proxy presented here will be beneficial in pinpointing the location and extent of OC release from thawing permafrost in the coastal or fluvial environment. With enhanced Arctic warming and associated intensification of permafrost thaw, constraining the amount and fate of permafrost OC release will help to assess the magnitude of the permafrost carbon feedback to climate warming." (lines 658-663).

Figure 2 – I would add the color legend to this figure that you already use on the other figures. I would also list n values in the caption or on the figure.

Yes, this has been changed.

Figure 5 - I would list the modern/ICD labels as headers rather than within the data.

OK, we have done this.

1 **Distinguishing between old and modern permafrost sources in the Northeast**
2 **Siberian land-shelf system with compound-specific $\delta^2\text{H}$ analysis**

3
4 Jorien E. Vonk¹, Tommaso Tesi^{2,3}, Lisa Bröder^{2,4}, Henry Holmstrand^{2,4}, Gustaf
5 Hugelius^{4,5}, August Andersson^{2,4}, Oleg Dudarev^{6,7}, Igor Semiletov^{6,7,8}, Örjan
6 Gustafsson^{2,4}

7
8 ¹ Department of Earth Sciences, VU University, The Netherlands

9 ² Department of Environmental Science and Analytical Chemistry, Stockholm
10 University, Sweden

11 ³ ISMAR Institute of Marine Sciences, Bologna, Italy

12 ⁴ Bolin Centre for Climate Research, Stockholm University, Sweden

13 ⁵ Department of Physical Geography, Stockholm University, Sweden

14 ⁶ Pacific Oceanological Institute FEBRAS, Vladivostok, Russia

15 ⁷ Tomsk Polytechnic University, Tomsk, Russia

16 ⁸ University of Alaska Fairbanks, Fairbanks, USA

17
18 Correspondence to: Jorien Vonk (j.e.vonk@vu.nl)

19
20
21 **Keywords:** deuterium isotopes, yedoma, ice complex deposit, n-alkanoic acids, n-
22 alkanes, organic matter, stable carbon isotopes, radiocarbon, Siberian Arctic,
23 sediments, permafrost thaw

24
25 **Abstract**

26 Pleistocene ice complex permafrost deposits contain roughly a quarter of the organic
27 carbon (OC) stored in permafrost terrain. When permafrost thaws, its OC is
28 remobilized into the (aquatic) environment where it is available for degradation,
29 transport or burial. Aquatic or coastal environments contain sedimentary reservoirs
30 that can serve as archives of past climatic change. As permafrost thaw is increasing
31 throughout the Arctic, these reservoirs are important locations to assess the fate of
32 remobilized permafrost OC.

33 We here present compound-specific deuterium ($\delta^2\text{H}$) analysis on leaf waxes as a tool
34 to distinguish between OC released from thawing Pleistocene permafrost (Ice
35 Complex Deposits; ICD) and from thawing Holocene permafrost (from near-surface
36 soils). Bulk geochemistry (%OC, $\delta^{13}\text{C}$, %total nitrogen; TN) was analyzed as well as
37 the concentrations and $\delta^2\text{H}$ signatures of long-chain *n*-alkanes (C_{21} to C_{33}) and
38 mid/long-chain *n*-alkanoic acids (C_{16} to C_{30}) extracted from both ICD-PF samples
39 ($n=9$) and modern vegetation/O-horizon (Topsoil-PF) samples ($n=9$) from across the
40 northeast Siberian Arctic.

41 Results show that these Topsoil-PF samples have higher %OC, higher OC/TN values,
42 and more depleted $\delta^{13}\text{C}$ -OC values than ICD-PF samples, suggesting that these former
43 samples trace a fresher soil and/or vegetation source. Whereas the two investigated
44 sources differ on the bulk geochemical level, they are, however, virtually
45 indistinguishable when using leaf wax concentrations and ratios.

Deleted: Median concentrations of high-molecular weight *n*-alkanes (sum of C_{25} - C_{27} - C_{29} - C_{31}) were 210 ± 350 $\mu\text{g/gOC}$ (median \pm IQR) for Topsoil-PF and 250 ± 81 $\mu\text{g/gOC}$ for ICD-PF samples. Long-chain *n*-alkanoic acids (sum of C_{22} - C_{24} - C_{26} - C_{28}) were more abundant than long-chain *n*-alkanes, both in Topsoil-PF samples (4700 ± 3400 $\mu\text{g/gOC}$) and in ICD samples (6630 ± 3500 $\mu\text{g/gOC}$).

53 However, on the molecular-isotope level, leaf wax biomarker $\delta^2\text{H}$ values are
54 statistically different between Topsoil-PF and ICD-PF. For example, the mean $\delta^2\text{H}$
55 value of C_{29} *n*-alkane was $-246 \pm 13\text{‰}$ (mean \pm stdev) for Topsoil-PF and $-280 \pm 12\text{‰}$
56 for ICD-PF. With a dynamic isotopic range (difference between two sources) of 34 to
57 50‰, the isotopic fingerprints of individual, abundant, biomarker molecules from
58 leaf waxes can thus serve as end-members to distinguish between these two sources.
59 We tested this molecular $\delta^2\text{H}$ tracer along with another source-distinguishing
60 approach, dual-carbon ($\delta^{13}\text{C}$ - $\Delta^{14}\text{C}$) isotope composition of bulk OC, for a surface
61 sediment transect in the Laptev Sea. Results show that general offshore patterns
62 along the shelf-slope transect are similar, but the source apportionment between the
63 approaches vary, which may highlight the advantages of either. This study indicates
64 that the application of $\delta^2\text{H}$ leaf wax values has potential to serve as a complementary
65 quantitative measure of the source and differential fate of OC thawed out from
66 different permafrost compartments.
67

Deleted: T

Deleted: , whereas the C_{31} *n*-alkane was $-247 \pm 23\text{‰}$ for Topsoil-PF and $-297 \pm 15\text{‰}$ for ICD-PF. The C_{28} *n*-alkanoic acid $\delta^2\text{H}$ value was $-220 \pm 15\text{‰}$ for Topsoil-PF and $-267 \pm 16\text{‰}$ for ICD-PF.

Deleted: The $\delta^2\text{H}$ molecular approach has the advantage that it circumvents uncertainties related to a marine end-member, yet the $\delta^{13}\text{C}$ - $\Delta^{14}\text{C}$ approach has the advantage that it represents the bulk OC fraction thereby avoiding issues related to the molecular-bulk upscaling challenge.

78 **1 Introduction**

79 Climate warming is causing permafrost soils to thaw, exposing its organic matter
80 (OM) to decomposition (e.g., Schuur et al., 2015; Zimov et al., 1993; Semiletov et al.,
81 2012). Thaw will increase the hydrological connectivity of landscapes and will cause
82 release of OM into the aquatic environment (Walvoord et al., 2012; Vonk et al., 2015;
83 Anderson et al., 2011). Here, the OM can continue to decompose, generating
84 greenhouse gases (e.g., Semiletov et al., 1996a,b; Anderson et al., 2009; Shakhova et
85 al., 2015), or be destined for burial in inland and coastal sediments. These
86 sedimentary archives serve as long- and short-term reservoirs that attenuate
87 greenhouse gas emissions from thawing permafrost (Vonk and Gustafsson, 2013;
88 Semiletov et al., 2011).

Deleted: to

89
90 The release of OM from thawing permafrost into aquatic sediments varies over time
91 and space. A recent study showed that at the end of the last glacial, the surface active
92 layer of terrestrial permafrost released about 4.5 Tg organic carbon (OC) per year
93 from just the Lena watershed onto the nearby shelf, whereas current annual OC
94 release is estimated to be only about a tenth of this (Tesi et al., 2016). In addition to
95 active layer material, OM from deeper and older permafrost sources can also thaw
96 and be released into the environment (Shakhova et al., 2007, 2014). This process
97 currently dominates the delivery of terrestrial material onto the East Siberian Arctic
98 shelf (Vonk et al., 2012; Semiletov et al., 1999) and is expected to increase due to
99 accelerating coastal erosion rates (Günther et al., 2013).

100
101 Different permafrost OC stocks exhibit variable vulnerabilities to thaw remobilization
102 (Schuur et al., 2015). In addition to a subsea permafrost OC stock, soils and sediments
103 of the terrestrial northern permafrost zone store about 1300±200 Pg OC, with
104 separate upscaling approaches applied for soil stocks (0-3m depth), deltaic sediments
105 (full depth) and Yedoma sediments (full depth) (Hugelius et al., 2014). Yedoma
106 sediments, a.k.a. Ice Complex Deposits (ICD) are polygenetic, ice-rich Pleistocene-
107 aged deposits that are present in the unglaciated parts of Siberia and Alaska
108 (Schirrmeister et al., 2011). These deposits contain roughly a quarter of the OC stored
109 in permafrost terrain, but estimates vary from ca. 200-400 Pg C (Strauss et al., 2013;
110 Schuur et al., 2015). The presence of massive ice wedges in ICD causes landscapes to
111 collapse upon thaw, exposing deeper stocks of OC. This type of relatively abrupt thaw
112 is increasing in many parts of the arctic landscape (Schuur et al., 2015). At the same
113 time, deepening of the active layer causes gradual thaw that occurs across entire
114 landscapes (Shiklomanov et al., 2013).

115
116 With a tool to detect and monitor different types of permafrost OM in coastal
117 environments, one could assess (historical and spatial) variability in permafrost
118 source input, degradation and thaw, as well as the relative degradation of different
119 permafrost types. For example, the relative release of OC from ICD versus topsoil
120 permafrost has earlier been distinguished and quantified through the use of dual-
121 carbon isotopes ($\delta^{13}\text{C}$ and $\Delta^{14}\text{C}$) on bulk OC in the shelf environment of the Laptev
122 and East Siberian Sea. It was shown that topsoil permafrost OC dominates in
123 suspended particulate matter (Karlsson et al., 2011; 2016; Vonk et al., 2012) and ICD

125 permafrost OC dominates in the surface sediments (Vonk et al., 2012; Semiletov et al.,
126 2011; 2012). Vonk et al. (2014) further showed that topsoil OC is actively degraded
127 during horizontal transport whereas ICD permafrost OC rapidly settles. Winterfeld et
128 al. (2015) showed, using dual-carbon isotopes on riverine material, that suspended
129 particulate OC in the Lena Delta mostly consists of Holocene material instead of
130 material from ICD permafrost.

131
132 This $\delta^{13}\text{C}$ - $\Delta^{14}\text{C}$ dual-carbon isotope approach carries the strong advantage that it
133 operates on the bulk OC level, thereby circumventing the "molecular-bulk upscaling
134 challenge". This challenge relates to issues associated with upscaling from the
135 molecular isotope level to the bulk level. These issues relate to the relative
136 concentration (*n*-alkanes and *n*-alkanoic acids represent only a fraction of the total
137 OC) but also to processes such as selective degradation, differences in physical
138 association, or dispersion differences. However, the $\delta^{13}\text{C}$ - $\Delta^{14}\text{C}$ approach also has
139 drawbacks, such as a weak distinction between the $\delta^{13}\text{C}$ end-member values of
140 Topsoil-PF versus ICD-PF. Also, the marine $\delta^{13}\text{C}$ end member values in coastal Arctic
141 shelf waters are uncertain and may be more depleted than at mid-latitudes due to
142 uptake of relatively depleted dissolved CO_2 values caused by cold polar water
143 (Meyers, 1997; Tesi et al. *this special issue*) or degradation of terrestrial matter
144 (Anderson et al., 2009; 2011; Semiletov et al., 2013; 2016), generating a potential
145 overlap between marine and topsoil $\delta^{13}\text{C}$ end-members.

146
147 Here we propose a complementary tool to trace permafrost OC release into the
148 coastal environment based on molecular $\delta^2\text{H}$ analysis on leaf waxes. We will evaluate
149 the performance of this tool using additional geochemical data as well as a bulk $\delta^{13}\text{C}$ -
150 $\Delta^{14}\text{C}$ mixing approach. Isotopes in water molecules ($\delta^2\text{H}$ or $\delta^{18}\text{O}$) in glacial ice cores
151 as well as in massive ground ice in the northern hemisphere have been used for
152 reconstructing palaeotemperatures (e.g., Kotler and Burn, 2000; Johnson et al., 2001;
153 Opel et al., 2011; Meyer et al., 2015; Wetterich et al., 2016) as the isotopic value of
154 local precipitation is a function of local climate (Craig, 1961; Sachse et al., 2004; Smith
155 and Freeman, 2006). Higher plants use water as their primary source of hydrogen
156 during photosynthesis (Sternberg, 1988). The $\delta^2\text{H}$ isotope values of leaf wax *n*-
157 alkanolic acids or *n*-alkanes are therefore reflecting the $\delta^2\text{H}$ isotopic value of local
158 precipitation (e.g., Sachse et al., 2004; Sessions et al., 1999), after correction for the
159 net fractionation during biosynthesis, and evapotranspiration (Leaney et al., 1985).
160 Global precipitation values can vary immensely (Dansgaard, 1964), with values up to
161 +50‰ in Eastern Africa but approaching -200‰ near the North Pole (www.iaea.org)
162 or even below -400‰ in Antarctica (i.e. SLAP2 standard, Standard Light Antarctic
163 Precipitation, is -427.5‰). Additionally, the fractionation between source water and
164 plant wax molecules varies both in time and space, and can be up to -170‰ (Smith
165 and Freeman, 2006; Sachse et al., 2004; Polissar and Freeman, 2010) but appears
166 relatively small at higher latitudes (between -59 and -96‰; Shanahan et al., 2013;
167 Wilkie et al., 2013; Porter et al., 2016). Differences in $\delta^2\text{H}$ signatures of leaf wax
168 molecules from terrestrial regions with different (past) climates could therefore
169 potentially be applied to derive the relative proportion of different types of thawing

Deleted: proxies
Formatted: Font:Italic
Formatted: Font:Italic
Deleted: that relate to upscaling from the molecular to the bulk level (e.g.
Deleted:)

Formatted: Font:12 pt
Deleted: by as much as 200‰
Formatted: Font:12 pt
Deleted: around
Deleted: 0
Deleted: the tropics

178 permafrost in nearby coastal settings. Despite the plant fractionation associated with
179 kinetics and plant physiology (Sachse et al., 2012), we hypothesize that $\delta^2\text{H}$
180 signatures of leaf wax *n*-alkanoic acids and *n*-alkanes are more depleted in OC from
181 permafrost deposits formed during the colder Pleistocene (generally correlating with
182 ^2H -depleted precipitation), compared to more enriched values in OC from active layer
183 or surface permafrost formed during the warmer Holocene.

Deleted: w

Deleted: and drier

Formatted: Superscript

184
185 This study investigates a source-specific $\delta^2\text{H}$ signature for both ICD permafrost and
186 recent, surface soil permafrost in Northeast Siberia. Furthermore, we explore the
187 possibilities of using these isotopic end-member values in regional source-
188 apportionment calculations that aim to quantify the relative contribution of different
189 sources of permafrost OC. As permafrost thaw progresses, particularly in ice-rich
190 permafrost such as ICD, it is increasingly important to trace the fate of remobilized
191 and decomposing OC in the Arctic environment. Our proposed tool may be used to
192 trace these temporal and spatial differences in OC release from permafrost thaw, as
193 well as the extent of burial of OC in sedimentary reservoirs.

195 2 Methods

197 2.1 Sampling

198 A total of 18 samples were collected throughout the Siberian Arctic. Recent surface
199 soils ($n=7$) and vegetation ($n=2$) samples were analyzed and (from here on) referred
200 to as the "topsoil" permafrost (Topsoil-PF) sample set, whereas ICD-PF samples were
201 obtained from ICD soil profiles ($n=7$) and suspended particulates from ICD
202 formations ($n=2$) (Fig. 1 and Table 1). Eight offshore sediments along a shelf-slope-
203 continental rise transect in the Laptev Sea were collected in 2014, further marine
204 sampling details can be found in Bröder et al. (2016b).

205
206 The Topsoil-PF samples represent O and A soil genetic horizons in sites with active
207 soil formation. The sites were chosen to represent typical soil and vegetation types
208 in the investigated permafrost landscapes, including both taiga and tundra sites.
209 Samples were collected by depth or soil horizon increments from open soil pits using
210 fixed volume sampling procedures.

211
212 The ICD-PF samples were collected from vertical exposures that were excavated to
213 expose intact permafrost. Fixed-volume samples were collected by coring
214 horizontally into the frozen sediments to extract ICD-PF samples from consecutive
215 depths.

216
217 For more details about sampling sites, including location, vegetation and soil types
218 see table 1 (terminology following the U.S.D.A. Soil Taxonomy; Soil Survey Staff,
219 2014). Sampling was done in late summer near the time of maximum annual active
220 layer depth, in July 2010 (ICD-8 and ICD-9; Vonk et al. (2013)) and August 2011
221 (Palmtag et al., 2015) for the Kolyma River region, in August 2012 for the lower Lena
222 River and Indigirka River (Siewert et al., 2015; Weiss et al., 2015) and in August 2013

Deleted: CH DY-3A and 4A

226 for the upper Lena River (Siewert et al., 2016). For more detailed descriptions of
227 sample collection we refer to these references. The vegetation samples **TS-8G (grass)**
228 and **TS-9G (grass)** were obtained from the tundra near Medvezhka River and a birch
229 forest near Y4 stream, respectively, in July 2012.

Deleted: CH

Deleted: Medv

Deleted: CH Y4

230
231 Samples **ICD-8** and **ICD-9** were obtained in July 2010 at the Duvannyi Yar ICD
232 exposure along the Kolyma River (Vonk et al., 2013). The particulate sediment
233 samples were taken from thaw streams that were freshly formed from thawing ICD
234 (transport time from thaw to sampling estimated to be less than 1h).

Deleted: CH DY-3A

Deleted: 4A

235 2.2 Analytical methods

236 Freeze-dried samples were extracted using an ASE 200 accelerated solvent extractor
237 (Dionex Corporation, USA) using DCM/MeOH (9:1 v/v) at 80°C (5x10⁶ Pa)
238 (Wiesenberg et al., 2004). After the extraction, solvent-rinsed activated copper and
239 anhydrous sodium sulfate were added to the extracts to remove sulfur and excess
240 water, respectively. After 24 h, extracts were filtered on pre-combusted glass wool
241 and concentrated with the rotary evaporator. Extracts were transferred into glass
242 tubes, evaporated to complete dryness and re-dissolved in 500 µl of DCM. Lipid
243 fractionation was performed via column chromatography using amino-propyl Bond
244 Elut (500 mg/3 ml) to retain the acid fraction and Al₂O₃ to separate the hydrocarbon
245 and polar fractions (Vonk et al., 2010).

246
247
248 Prior to the analyses, saturated *n*-alkanes (hydrocarbon fraction) were further
249 purified using 10% AgNO₃ coated silica gel to retain the unsaturated fraction. The acid
250 fraction was methylated using a mixture of HCl, MilliQ water and methanol at 80°C
251 overnight to obtain the fatty acid methyl ester (FAME) fraction. Methylated acids
252 were extracted with hexane and further purified using 10% AgNO₃ coated silica gel.
253 The hydrocarbon and FAME fractions were quantified via gas chromatography mass
254 spectrometry (GC-MS) in full scan mode (50-650 m/z) using the response factors of
255 commercially available standards (Sigma-Aldrich). The GC was equipped with a 30
256 m×250 µm DB5-ms (0.25 µm thick film) capillary GC column. Initial GC oven
257 temperature was set at 60°C followed by a 10°C min⁻¹ ramp until a final temperature
258 of 310°C (hold time 10 min).

259
260 The hydrogen-isotopic composition of hydrocarbon and FAME fractions was
261 measured with continuous-flow GC - isotope ratio - MS. Purified extracts were
262 concentrated and injected (1-2 µl) into a Thermo Trace Ultra GC equipped with a
263 30m×250 µm HP5 (0.25 µm thick film) capillary GC column. Oven conditions were
264 similar to the setting used for the quantification. The conversion of organic
265 biomarkers to elemental hydrogen was accomplished by high-temperature
266 conversion (HTC) at 1420°C (Thermo GC Isolink). After the HTC, H₂ was introduced
267 into the isotope ratio MS (Thermo Scientific™ Delta V™IRMS) for compound-specific
268 determination of δ²H values via a Thermo ConFlo IV. Following a linearity test, we only
269 used peaks with amplitude (mass 2) between 1500 and 8000 mV for the evaluation.
270 The δ²H values were calibrated against saturated HMW *n*-alkanes using the reference

276 substance mix A4 (Biogeochemical Laboratories, Indiana University). The H_3^+ factor
277 (Sessions et al., 2001) was determined every day and stayed constant ($<3\text{‰}/V$)
278 throughout our analyses period. Each purified extract was injected three times.
279 FAMES were further corrected to account for the methylation agent by comparing the
280 hydrogen abundance of lauric acid (C_{12} -FA; i.e. 12 carbon atoms) as acid and
281 corresponding methyl ester. The average methylation correction for lauric acid was
282 $23.97 \pm 3.9\text{‰}$ ($n=4$). This correction was, normalized to chain length (i.e. increasing
283 chain lengths result in lower corrections), applied to all the FAMES. δ^2H values of n -
284 alkanes and FAMES are reported as mean, standard deviation and weighted average,
285

Formatted: Subscript

Formatted: Superscript

Deleted: the evaluation

Deleted: effect

Deleted: factor

Deleted: (Table 5)

286 Details of the analytical methods for extraction, work-up, and purification of the eight
287 offshore sediment samples for biomarker analysis that are included in our source-
288 apportionment comparison (section 4.3) can be found in Bröder et al. (2016b). The
289 δ^2H analysis on the shelf sediments was performed in parallel with the ICD-PF and
290 Topsoil-PF samples, according to the method described above.
291

Formatted: Font:Symbol

Formatted: Superscript

292 2.3 Source apportionment

293 The compound-specific δ^2H signatures in this study were used to differentiate
294 between the two major sources (end-members), Topsoil-PF and ICD-PF, using an
295 isotopic mass-balance model. We used a Markov chain Monte Carlo (MCMC) approach
296 to account for the end-member variability (Andersson et al., 2015; Bosch et al., 2015).
297 The end-members were represented by normal distributions, with mean and
298 standard deviations obtained from our analysis (δ^2H on TS and ICD samples) and
299 from literature ($\delta^{13}C$ and $\Delta^{14}C$ on end-members). For each Laptev Sea station, the
300 isotope signatures from three different terrestrial molecular markers (long-chain n -
301 alkanes C_{27} , C_{29} and C_{31}) were used jointly to improve source apportionment
302 precision. The δ^2H signatures for the two end-members were based on our Topsoil-
303 PF and ICD-PF samples,
304

Formatted: Font:12 pt

Formatted: Font:Symbol, 12 pt

Formatted: Font:12 pt, Superscript

Formatted: Font:12 pt

Formatted: Font:Symbol, 12 pt

Formatted: Font:12 pt, Superscript

Formatted: Font:12 pt

Deleted: from the literature values

Formatted: Font:Symbol, 12 pt

Formatted: Font:12 pt, Superscript

Formatted: Font:12 pt

Deleted: (see Table 5 for mean source values)

305 The compound-specific δ^2H -based source apportionment was compared to
306 $\Delta^{14}C/\delta^{13}C$ -based analysis of bulk OC using analogous MCMC techniques (e.g., Vonk et
307 al., 2012). The $\Delta^{14}C/\delta^{13}C$ -approach allows estimation of the relative contribution of a
308 third source, marine, which does not affect the presently investigated (terrestrial)
309 compounds. Accounting for the marine component to OC allows direct comparison of
310 the Holocene and Pleistocene contributions. All MCMC calculations were made using
311 Matlab scripts (ver. 2014b) using 200,000 iterations, a burn-in phase (initial search
312 period) of 10,000 and a data thinning of 10.
313

314 The spatial extent of ICD in the Lena River Basin was calculated by overlaying
315 the extent of the drainage basin (from WRIBASIN: Watersheds of the World
316 published by the World Resources Institute, [www.wri.org/publication/watersheds-
317 world](http://www.wri.org/publication/watersheds-world)) with the extent of the Yedoma Region (digitized from Romanovsky, 1993) in
318 an equal area map projection. It was assumed that 30% of the Yedoma Region consists
319 of intact ICD (following Strauss et al., 2013).
320

327 **3 Results**

329 **3.1 Bulk geochemistry**

330 The investigated Topsoil-PF and ICD-PF samples are, on a bulk geochemical level,
331 very different. Mean organic carbon contents (as %OC) and total nitrogen content (as
332 %TN) are 25±12 and 1.1±0.67 for Topsoil-PF samples, and 1.6±0.31 and 0.17±0.058
333 for ICD-PF samples, respectively (Table 1). This gives TOC/TN ratios of 25±8.0 for
334 Topsoil-PF samples and 10±2.6 for ICD-PF samples. Stable carbon isotopic values of
335 Topsoil-PF and ICD-PF samples are -27.8±1.3‰ and -25.7±0.75‰, respectively
336 (Table 1).

338 **3.2 Molecular geochemical composition**

339 Long-chain *n*-alkanes and *n*-alkanoic acids are abundant in epicuticular waxes and
340 therefore indicative for a source of higher plants (Eglinton and Hamilton, 1967).
341 Concentrations of individual long-chain *n*-alkanes in Topsoil-PF samples ranged from
342 1 to 340 µg/gOC (C₂₁-C₃₃; Table 2) with an average chain length of 28±1.6. The sum
343 of high-molecular weight (HMW) *n*-alkanes (>C₂₁) for Topsoil-PF samples was
344 418⁶¹²₂₈₀ µg/gOC (median with interquartile range) and the most abundant *n*-alkanes
345 added up to 214⁴⁹⁴₁₄₈ µg/gOC (sum of C₂₅-C₂₇-C₂₉-C₃₁) (Table 4, Fig. 2a). For ICD-PF
346 samples, the individual concentrations of long-chain *n*-alkanes were between 4 and
347 160 µg/gOC, and the average chain length 27±0.7 (Table 2). The sum of high-
348 molecular weight *n*-alkanes, and most abundant *n*-alkanes were 698⁸⁰⁶₆₃₀ µg/gOC and
349 347⁴⁰⁵₃₂₃ µg/gOC, respectively (Table 4, Fig. 2a). The carbon preference index (CPI), a
350 molecular ratio indicative for degradation status with values >5 typical for fresher
351 terrestrial material and values approaching 1 typical for more degraded samples
352 (Hedges and Prahl, 1993), showed values for Topsoil-PF samples of 7.3±3.6
353 (average±standard deviation) and ICD-PF samples of 3.6±0.8 (CPI C₂₃-C₃₁; Table 4,
354 Fig. 2c). The C₂₅/(C₂₅+C₂₉) ratio, indicative for the input of peat moss (*Sphagnum* sp.)
355 material (Vonk and Gustafsson, 2009; *Sphagnum* values 0.72, higher plants 0.07; Nott
356 et al., 2000) was 0.33±0.22 (average±standard deviation) and 0.34±0.05 for Topsoil-
357 PF and ICD-PF samples, respectively (Table 4). Another commonly used *Sphagnum*
358 proxy (Bush and McInerney, 2013), C₂₃/(C₂₃+C₂₉), resulted in a sharper contrast
359 between ICD-PF and Topsoil-PF samples (0.39±0.13 and 0.25±0.23, respectively; Fig.
360 2e and Table 4).

361 Long-chain *n*-alkanoic acids (C₂₂ and above) were abundant in concentrations
362 between 0.122 and 2670 µg/gOC for individual homologues in topsoils, with the sum
363 of HMW *n*-alkanoic acids (>C₂₂) being 6397⁷⁴⁵⁴₃₁₆₇ µg/gOC (median and IQR), and the
364 most abundant *n*-alkanoic acids (sum of C₂₂-C₂₄-C₂₆-C₂₈) adding up to
365 4700⁶⁰⁹²₂₆₇₀ µg/gOC (Table 3, 4 and Fig. 2b). ICD-PF samples contained individual long-
366 chain *n*-alkanoic acids in 2.17 and 18700 µg/gOC (Table 2), a sum of HMW *n*-alkanoic
367 acids of 8290¹¹⁴³⁰₆₂₉₀ µg/gOC, and the sum of most abundant, even *n*-alkanoic acids of
368 6630⁸⁷⁹⁰₅₂₈₅ µg/gOC (Table 4). Topsoil-PF and ICD-PF samples had average chain lengths
369 of 24.1±1.1 and 24.3±0.59, and CPI (C₂₂-C₂₈) values of 5.9±2.7 (average±standard
370 deviation) and 5.0±1.6, respectively (Table 4). Shorter-chain *n*-alkanoic acids C₁₆ and
371

Deleted: 420±330 µg/gOC
Deleted: (median±IQR; interquartile range)
Deleted: to 210±350 µg/gOC

Deleted: were 700±180 µg/gOC
Deleted: and 350±81 µg/gOC

Formatted: Font:Italic
Formatted: Subscript
Formatted: Subscript
Formatted: Subscript
Deleted: .

Deleted: being 6400±4300 µg/gOC (median±IQR)

Deleted: to 4700±3400 µg/gOC
Deleted: 2
Deleted: 3
Deleted: of 8300±5100 µg/gOC, and the sum of most abundant, even *n*-alkanoic acids of 6600±3500 µg/gOC

384 C₁₈ are produced in basically all types of life in soils or aquatic environments, and are
385 not specific for higher plants. Topsoil-PF contained C₁₆ and C₁₈ homologues in
386 concentrations between 220 and 4600 µg/gOC, and ICD-PF samples between 200 and
387 10400 µg/gOC (Table 3).

388
389 Degradation of organic matter involves the loss of functional groups, e.g. the loss of
390 carboxylic acids (Meyers and Ishiwatari, 1993). A high ratio of HMW *n*-alkanoic acids
391 over HMW *n*-alkanes in a sample therefore implies a relatively fresh, less degraded,
392 status (i.e. relatively more functional groups present). For Topsoil-PF samples, the
393 HMW *n*-alkanoic acid/HMW *n*-alkane ratio varied between 5.6 and 25 with an
394 average value of 13±7.6, whereas ICD-PF samples varied between 7.6 and 140 with
395 an average value of 29±43 (Table 4, Fig. 2f).

396 397 **3.3 Molecular isotopic composition**

398 We measured δ²H values in long-chain *n*-alkanes and *n*-alkanoic acids between -119
399 and -313‰ (Fig. 3, Table 5). Mean values for HMW *n*-alkanes (C₂₅-C₂₇-C₂₉-C₃₁) were
400 between -201 and -247‰ for Topsoil-PF samples and between -221 and -297‰ for
401 ICD-PF samples, with consistently lower δ²H for longer chain lengths. For HMW *n*-
402 alkanoic acids (C₂₂-C₂₄-C₂₆-C₂₈) mean δ²H values were between -203 and -236‰ for
403 Topsoil-PF samples and between -261 and -278‰ for ICD-PF samples (Table 5). The
404 decrease in δ²H values with increasing chain length is less distinct for *n*-alkanoic acids
405 but one can observe a decrease of around 25-30‰ from C₂₂ to C₂₆ (Fig. 3). For ICD-
406 PF samples, the isotopic depletion for the average of the three most abundant *n*-
407 alkanes is comparable to the average for *n*-alkanoic acids, whereas in Topsoil-PF
408 samples, the isotopic depletion for the three most abundant *n*-alkanes is a bit larger
409 than for *n*-alkanoic acids (Fig. 4).

410 411 **4 Discussion**

412 413 **4.1 Using bulk geochemistry and molecular proxies**

414 Bulk geochemical and isotopic analysis, as well as analysis of molecular proxies
415 remained inconclusive in distinguishing between the two investigated sources in this
416 study. Topsoil-PF samples have a higher organic content, higher TOC/TN values
417 (representing fresh, higher plant material; Meyers, 1994) and more depleted δ¹³C
418 values (indicative for terrestrial C3 plants; Meyers, 1997) than ICD-PF samples,
419 suggesting that these samples indeed trace a fresh soil and/or vegetation source
420 (Table 1). The δ¹³C values of a larger ICD-PF and Topsoil-PF dataset have earlier been
421 summarized (Vonk et al., 2012 and references therein; Schirrmeister et al., 2011)
422 giving values of -26.3±0.67‰ (n=374) and -28.2±2.0‰ (n=30), respectively. Our
423 values (Table 1) are in a similar range. Despite the differences between these two
424 sources in their bulk geochemistry, it is hard to use these parameters for source
425 distinction as their variability is fairly high, and their behavior in the environment is
426 not conservative, but e.g. affected by degradation processes. On a molecular
427 geochemical level the two investigated sources are virtually indistinguishable as
428 there is a considerable variation in molecular concentrations and proxy values (Fig.

Deleted: it seems that

Deleted: h

431 2). Only one of the tested parameters, the CPI C_{23} - C_{31} of *n*-alkanes, showed a
432 statistically significantly different value for the two investigated sources.
433

434 4.2 Evaluation of molecular δ^2H values as a source end-member

435 To alleviate the difficulty to distinguish between Topsoil-PF and ICD-PF with just bulk
436 and molecular geochemical characteristics, we explore the δ^2H values of leaf wax
437 molecules (i.e. long chain *n*-alkanoic acids and *n*-alkanes) to differentiate between
438 their relative source contributions. The overall mean δ^2H of the four most abundant
439 *n*-alkanoic acids is $-231\pm 29\text{‰}$ and $-271\pm 13\text{‰}$ for Topsoil-PF and ICD-PF samples,
440 respectively. These values compare well with available literature (Fig. 5). Pautler et
441 al. (2014) measured δ^2H values on C_{29} *n*-alkanes in modern soils of the Yukon, Canada
442 of $-252\pm 9.1\text{‰}$ ($n=4$) and aged soil δ^2H values of $-269\pm 8.6\text{‰}$ ($n=13$; 24-25 ^{14}C -ka ago)
443 and $-273\pm 16.4\text{‰}$ ($n=9$; for MIS 4, ~ 70 ^{14}C -ka ago). Yang et al. (2011) also reported
444 C_{29} *n*-alkane δ^2H values for modern vegetation from Alaska and Arctic Canada with an
445 average value of $-252\pm 43\text{‰}$ ($n=8$). Zech et al. (2011) reported values of C_{29} *n*-alkanes
446 collected from a permafrost exposure along the Tumara River in northeast Siberia,
447 with an average value of $-266\pm 7.5\text{‰}$ ($n=23$) for glacial paleosoils and $-247\pm 9.4\text{‰}$
448 ($n=17$) for interglacial paleosoils. Our values for C_{29} *n*-alkanes for Topsoil-PF ($-$
449 $246\pm 13\text{‰}$; $n=9$) and ICD-PF ($-280\pm 12\text{‰}$; $n=9$) are in a similar range (Fig. 5). For C_{28}
450 *n*-alkanoic acids, Wilkie et al. (2013) measured $-252\pm 8.7\text{‰}$ ($n=6$) for modern
451 vegetation in northeast Siberia, whereas Porter et al. (2016) measured $-269\pm 2.7\text{‰}$
452 ($n=7$) for ca. 31 cal ka BP old soils in the Yukon. Compared to these studies, our values
453 for C_{28} *n*-alkanoic acids are somewhat more enriched for Topsoil-PF with $-220\pm 15\text{‰}$
454 ($n=7$) but roughly in the same range for ICD-PF with $-267\pm 16\text{‰}$ ($n=9$).
455

456 The mean isotopic difference between the most abundant *n*-alkanoic acids of the two
457 investigated sources is around 40‰ (δ^2H values of $-231\pm 29\text{‰}$ and $-271\pm 13\text{‰}$ for
458 Topsoil-PF and ICD-PF samples, respectively). Despite the relatively large standard
459 deviations, the isotopic differences are statistically significant for each of the *n*-
460 alkanoic acids individually (C_{22} , C_{24} , C_{26} , C_{28} ; Fig. 3). The isotopic differences between
461 the two sources for the mean value of the four most abundant *n*-alkanes is 35‰, with
462 a mean value of $-229\pm 33\text{‰}$ and $-264\pm 34\text{‰}$ for Topsoil-PF and ICD-PF samples,
463 respectively. Here, the individual *n*-alkane isotopic signatures are statistically
464 significantly different for C_{27} , C_{29} , C_{31} (Fig. 3) in Topsoil-PF and ICD-PF samples. The
465 selection and application of individual chain length δ^2H values as end-members, in
466 contrast to mean chain length values, might be more appropriate for several reasons;
467 (i) to reduce variability (δ^2H ranges for C_{29} and C_{31} *n*-alkanes and C_{22} and C_{24} *n*-
468 alkanoic acids are relatively low; Fig. 3), (ii) to target the most abundant species (C_{29}
469 and C_{31} *n*-alkanes are generally more abundant in soils and ICD-PF compared to
470 shorter chain lengths; Table 2), and (iii) to make use of the largest dynamic range
471 between source end-member values (C_{31} *n*-alkane δ^2H values of Topsoil-PF and ICD-
472 PF differ by 50‰). Based on these arguments, the C_{28} *n*-alkanoic acid and the C_{29} or
473 C_{31} *n*-alkanes are most appropriate to use for source-apportionment. The available
474 previous studies (Fig. 5) have also selected these chain lengths (C_{28} *n*-alkanoic acid
475 and C_{29} *n*-alkanes) for proxy development.

476
477 The use of molecular $\delta^2\text{H}$ values as tracers of terrestrial material in a marine or
478 coastal setting has the advantage that it avoids uncertainty issues related to definition
479 of the marine end-member. On the other hand, the inherent bulk-upscaling challenge
480 of any molecular proxy is a disadvantage of the $\delta^2\text{H}$ approach as it introduces
481 unknowns related to the molecular-bulk upscaling effort (e.g. taking into account
482 sorting and recalcitrance; discussed in depth in 4.3). We also want to emphasize that
483 $\delta^2\text{H}$ leaf wax values in the two studied end-member sets (Topsoil-PF vs. ICD-PF)
484 largely depend on the climate (warm vs. cold) and continentality (near the coast vs.
485 further inland) during plant formation, and associated differences in fractionation
486 mechanisms. Consequently, when $\delta^2\text{H}$ values in samples are used for source-
487 apportionment, this may represent the fraction leaf wax produced in cold vs. warm
488 conditions (as well as degree of continentality), and not necessarily the fraction
489 Topsoil-PF vs. ICD-PF.

Deleted: ies

490
491 Finally, we realize that the amount of soil and ICD samples analyzed in this study is
492 limited, and want to point out that the results may change when more data are
493 analyzed in the near future. Additionally, studies have shown that the $\delta^2\text{H}$ signature
494 of ice within ICD permafrost deposits can range from roughly -150‰ to -260‰
495 depending on the type of ice (wedge ice vs. pore or texture ice) as well as the period
496 of formation (different Pleistocene cold stages) (Opel et al., 2017 and references
497 therein). The source of water (i.e. type of ice) and age of the deposit will therefore
498 influence the *n*-alkane or *n*-alkanoic acid $\delta^2\text{H}$ signal. However, regardless of the
499 natural variability associated with the processes mentioned above, both ICD and
500 texture-ice isotopic compositions appear to reflect long-term climate changes (Opel
501 et al., 2017; Schwamborn et al., 2006; Dereviagin et al., 2013; Porter et al., 2016)
502 which, likely, were also captured in the *n*-alkane or *n*-alkanoic acid $\delta^2\text{H}$ signal.
503 Unfortunately, we do not have ^{14}C -ages available for all ICD samples, so cross-
504 referencing to published stratigraphies in the region is not possible. Coastal
505 sediments, however, will represent a mixture of material released from different
506 depths, outcrops, and stratigraphies within the catchment or coast. For source-
507 apportionment applications, we reason that a growing body of leaf wax $\delta^2\text{H}$ end-
508 member data from the ICD region can overcome the variability issues highlighted
509 above.

Deleted: -

510 511 **4.3 Comparison with ^{13}C - ^{14}C source-apportionment: a case-study**

512 Bulk OC dual-carbon isotope data provide a quantitative apportionment tool to assess
513 the relative contributions of Topsoil-PF vs. ICD-PF. Here, we present a case-study of
514 a shelf-slope transect in the Laptev Sea (Fig. 1) where both these source-
515 apportionment tools for the first time can be applied, compared and evaluated. The
516 shelf-slope transect of eight surface sediment samples stretches over 600 km from
517 the nearshore zone (72.7°N, <10m water depth) to the continental rise (78.9°N,
518 >3000m depth) (Table 6). More molecular and bulk geochemical characteristics of
519 these samples can be found in Bröder et al. (2016b).

520

523 The $\delta^{13}\text{C}$ - $\Delta^{14}\text{C}$ source-apportionment uses three end-members (marine, Topsoil-PF,
524 and ICD-PF). End-member values are based on previously published values (Tesi et
525 al., 2016); with a $\delta^{13}\text{C}$ value of $-27.0\pm 1.2\text{‰}$ (n=38; Rodionow et al., 2006; Tesi et al.,
526 2014; Gundelwein et al., 2007; Bird et al., 2002) for Topsoil-PF, and $-26.3\pm 0.67\text{‰}$
527 (n=374; Vonk et al., 2012; Schirrmeister et al., 2011) for ICD-PF. The Topsoil-PF $\Delta^{14}\text{C}$
528 endmember was defined as $-232\pm 147\text{‰}$ (n=29; Winterfeld et al., 2015; Jasinski et al.,
529 1998; Kaiser et al., 2007; Höfle et al., 2013; Palmtag et al., 2015). For ICD-PF we used
530 a $\Delta^{14}\text{C}$ value of $-940\pm 84\text{‰}$ (n=300; Vonk et al., 2012 and references therein). The
531 marine end-member value was $-21.0\pm 2.6\text{‰}$ (n=10; Panova et al., 2015) and $-$
532 $50.4\pm 12\text{‰}$ (n=10; Panova et al., 2015) for $\delta^{13}\text{C}$ and $\Delta^{14}\text{C}$, respectively. Calculations
533 were made using a Markov chain Monte Carlo approach (see 2.3).
534

535 For $\delta^2\text{H}$ source-apportionment there is no need to include a marine end-member as
536 marine organisms do not produce long-chain *n*-alkanes or *n*-alkanoic acids. We were
537 unfortunately only able to analyze *n*-alkanes in the shelf-slope transect samples, and
538 no *n*-alkanoic acids, due to limitations in sample volume. We used the $\delta^2\text{H}$ values of
539 the C_{27} , C_{29} and C_{31} *n*-alkanes, individually. In other words, these three chain lengths
540 are taken as independent markers, providing an overdetermined system (i.e. two
541 sources defined with three different markers). This is more representative than using
542 the average (concentration-weighted) $\delta^2\text{H}$ value for these *n*-alkanes as the end-
543 member values for each chain length are different. For Topsoil-PF we used $-$
544 $215\pm 39\text{‰}$, $-246\pm 13\text{‰}$, and $-247\pm 23\text{‰}$ for C_{27} , C_{29} and C_{31} *n*-alkanes, and for ICD-PF
545 we applied $-259\pm 18\text{‰}$, $-297\pm 15\text{‰}$, and $-282\pm 13\text{‰}$ for C_{27} , C_{29} and C_{31} *n*-alkanes,
546 respectively (see also Table 5). Afterwards, we averaged the three end-member
547 contributions derived from the three calculations for each station, thereby taking the
548 variability introduced by the end-members into account.
549

550 The source apportionment of OC from Topsoil-PF and ICD-PF to surface sediments
551 along the Laptev Sea transect differ between the bulk $\delta^{13}\text{C}$ - $\Delta^{14}\text{C}$ and leaf wax $\delta^2\text{H}$
552 approaches (Table 6). The former approach suggests Topsoil-PF contributions
553 between 21-70%, generally decreasing offshore, and, consequently, ICD-PF
554 contributions of 30-79%, generally increasing offshore. The latter (leaf wax $\delta^2\text{H}$)
555 approach results in a more extreme division of sources with Topsoil-PF contributions
556 of 83-91% and ICD-PF contributions of 9-17%, with similar patterns nearshore and
557 offshore (Table 6). A contribution of 9-17% may seem more in line with the estimated
558 extent of ICD in the Lena River basin: 12% of the basin falls within the Yedomia Region
559 (as defined by Romanovsky, 1993) and about 3% consists of intact ICD (see section
560 2.3). However, the cross-shelf sites are also strongly influenced by coastal and/or
561 subsea erosion (Karlsson et al. 2011; Vonk et al., 2012; Semiletov et al., 2012; 2016)
562 so the catchment characteristics are only one part of the story. It is challenging to
563 interpret the differences between the two proxies but we elaborate below on
564 potential reasons.
565

566 Assumptions in the bulk $\delta^{13}\text{C}$ - $\Delta^{14}\text{C}$ approach may affect these results. First, the
567 outcome of the bulk $\delta^{13}\text{C}$ - $\Delta^{14}\text{C}$ approach is sensitive to the definition of the marine

568 end-member. Changes in the currently used $\delta^{13}\text{C}$ and $\Delta^{14}\text{C}$ value of the marine end-
569 member of the East Siberian Arctic Shelf ($n=10$; Panova et al., 2015) would likely alter
570 the relative Topsoil-PF and ICD-PF contributions. The currently used standard
571 deviation for the $\delta^{13}\text{C}$ marine end-member is 2.6‰, which is much higher than the
572 values for the terrestrial end-members. Second, lateral transport time enroute the
573 shelf-slope transect (>600 kilometers) causing potentially significant aging of
574 sediments and its organic carbon is not accounted for in the source-apportionment.
575 Lateral transport time results in older surface OC ages on the shelf, compared to those
576 at the initial coastal deposition. Without correcting for this factor, the source-
577 apportionment will generate lower contributions of the (younger) Topsoil-PF
578 component. In an attempt to estimate this effect, we recalculated (similar to Bröder
579 et al. 2016a) the relative source contributions of Topsoil-PF, ICD-PF (and marine)
580 with the bulk $\delta^{13}\text{C}$ - $\Delta^{14}\text{C}$ approach with the assumption that the Topsoil-PF ^{14}C age
581 would be subject to a cross-shelf lateral transport time of 5000 yrs. We assumed a
582 linear aging along the transect based on distance from the coast, with a maximum
583 value of 5000 yrs aging at station SW-01. This resulted in Topsoil-PF contributions
584 that were up to 20% higher (for the deepest stations) compared to the source-
585 apportionment where lateral transport time was unaccounted for (Table 6; Fig. 6).
586

587 Assumptions in the leaf wax $\delta^2\text{H}$ source-apportionment approach could potentially
588 also impact the outcomes, and hence differences with the bulk $\delta^{13}\text{C}$ - $\Delta^{14}\text{C}$ results. First,
589 there is an inherent assumption related to the molecular to bulk level upscaling
590 challenge. We assume that the physical association of *n*-alkanes in different source
591 end-members (Topsoil-PF vs. ICD-PF) as well as their fractionation in the coastal
592 system is similar. However, previous research has shown that *n*-alkanes behave
593 rather differently upon their release into coastal waters; *n*-alkanes originating from
594 surface soil or vegetation debris are not bound to minerals and remain in suspension
595 during transport while being actively degraded, whereas *n*-alkanes originating in
596 deeper mineral soils settle quickly and are protected from extensive degradation
597 (Vonk et al., 2010). It is possible that most of the *n*-alkanes in the Laptev Sea sediment
598 transect originate in (deeper) mineral soils. An effect of physical association, as well
599 as the potential effect of hydrodynamic sorting patterns (Tesi et al., 2016) on the leaf
600 wax $\delta^2\text{H}$ values of both sources could impact the source-apportionment. Another
601 factor that can introduce a bias in our leaf wax $\delta^2\text{H}$ approach is a proton exchange of
602 the C-bound H-atoms in *n*-alkanes with environmental water, either from in situ
603 sources (soil water) or during transport (river or ocean water, or sediment pore
604 water). As there is no evidence for such exchange in young (<1 million years), cold
605 sediments (Sessions et al., 2004) we suspect this process may be minimal in our
606 samples (and end-members).
607

608 When accounting for an estimated lateral transport time, the difference in estimates
609 of source contribution by the two different approaches (bulk $\delta^{13}\text{C}$ - $\Delta^{14}\text{C}$ and leaf wax
610 $\delta^2\text{H}$) increases offshore, from about a 25% difference near the coast to a 40%
611 difference at stations SW-01 and SW-03. This increasing offset between the results of
612 the two end-member mixing methods may be caused by several factors such as

Deleted: Although t

Deleted: this process could be enhanced in environments of low pH. The precise effect of such exchange on the $\delta^2\text{H}$ signal of our samples (or end-members) is unknown, but we

618 variability in the marine end-member (e.g. due to changes in seasonal ice cover), a
619 selective degradation (of the topsoil OC) enroute that introduces a source bias or
620 isotopic fractionation, or remaining factors related to the lateral transport time
621 (incorrect assumption of 5000 years, non-linear aging along transect). These
622 differences highlight that both source-apportionment tools still could be fine-tuned
623 further by (i) increasing the sample size of sources to reduce end-member
624 uncertainties, (ii) continuous adjustments in end-member values and Markov chain
625 Monte Carlo calculations based on latest knowledge, and (iii) assuring regional
626 testing and verification of the method when applied to new environments.

627 5 Conclusions

628 Leaf wax $\delta^2\text{H}$ values in samples from aquatic recipient environments can be used to
629 source-apportion the incoming terrestrial OC into two end-members; a Pleistocene
630 ICD permafrost source and a younger, Holocene, topsoil source. Mean isotopic values
631 of the C_{29} *n*-alkane, C_{31} *n*-alkane, and C_{28} *n*-alkanoic acid showed a dynamic,
632 statistically significant range of 34, 50 and 46‰ between Topsoil-PF and ICD-PF
633 samples, respectively, with ICD-PF samples being consistently more depleted
634 indicative of formation during the colder and drier Pleistocene.

635
636
637 A case-study where we tested two isotopic proxies (leaf wax $\delta^2\text{H}$ and bulk $\delta^{13}\text{C}-\Delta^{14}\text{C}$)
638 to calculate the relative terrestrial source contribution of Topsoil-PF and ICD-PF
639 along a Laptev Sea surface sediment transect, showed that the two proxies yield
640 variable results but overall generate similar trends offshore. We reason that
641 variability is caused by factors such as lateral transport time, remaining uncertainties
642 in end-member definition, or environmental factors such as physical association.

643
644 Both methods (leaf wax $\delta^2\text{H}$ and bulk $\delta^{13}\text{C}-\Delta^{14}\text{C}$) bring along their inherent
645 disadvantages and advantages. The molecular approach has the distinct advantage
646 that it circumvents the uncertainties that are associated with marine end-member
647 definition in the case of bulk OC mixing model analysis. However, application of
648 molecular $\delta^2\text{H}$ in source-apportionment studies brings along challenges related to the
649 molecular-bulk upscaling step. Bulk $\delta^{13}\text{C}-\Delta^{14}\text{C}$ source-apportionment, on the other
650 hand, has the advantage to operate on a bulk and perhaps more representative level,
651 but is hampered by remaining uncertainties associated with the marine end-member.

652
653 This study shows that $\delta^2\text{H}$ of leaf wax molecules has the potential to be used in
654 quantitative source-apportionment studies of thawing permafrost in coastal or
655 marine settings. It can serve as an alternative or complementary approach to the
656 commonly applied bulk $\delta^{13}\text{C}-\Delta^{14}\text{C}$ method. We recommend continuing data collection
657 and optimization of end-member definition and calibration. Refining the molecular
658 $\delta^2\text{H}$ proxy presented here will be beneficial in pinpointing the location and extent of
659 OC release from thawing permafrost in the coastal or fluvial environment. With
660 enhanced Arctic warming and associated intensification of permafrost thaw,
661 constraining the amount and fate of permafrost OC release will help to assess the
662 magnitude of the permafrost carbon feedback to climate warming.

Formatted: Font:Symbol

Formatted: Superscript

Deleted: in order to increase our understanding of the fate of

665

666 **Data availability**

667 All data are available in Tables 1 through 6, as well as Supplementary Table S1.

668

669 **Acknowledgements**

670 We would like to acknowledge Robert Spencer, Sergey Davydov, Anya Davydova,
671 Ekatarina Bulygina, Peter Kuhry, Matthias Siewert, Juri Palmtag, Niels Weiss, Martin
672 Kruså, Volker Brüchert, Pete Hill, Vladimir Mordukhovich, Alexander Charkin, Deniz
673 Kosmach, Per Andersson, and sampling crew and personnel of IB Oden and RV Yakob
674 Smirnitskiy for help with sample collection in the field. Financial support has been
675 provided by the Dutch NWO (Veni #863.12.004), US-NSF (Polaris Project #1044610),
676 the Bolin Centre for Climate Research, the Knut and Alice Wallenberg Foundation
677 (SWERUS-C3 Program; KAW #2011.0027), the Swedish Research Council (VR #621-
678 2004-4039 and 621-2007-4631), the Russian Science Foundation (#15-17-20032 to
679 O. D.), the Nordic Council of Ministers Cryosphere-Climate-Carbon Initiative (project
680 Defrost, #23001), the European Research Council (ERCAdG project CC-TOP #695331
681 to Ö.G.). This study was supported by the Delta Facility of the Faculty of Science,
682 Stockholm University. GH would like to acknowledge funding from ESF-CryoCarb and
683 EU FP7-PAGE21 projects for topsoil and ICD sample collection. [The ISMAR
684 publication ID is #1931.](#)

685

686 **Author contributions**

687 Land-based samples were collected by GH and JEV, ship-based samples were
688 collected by IS, OD, ÖG, TT, LB, and JEV. Laboratory analysis was performed by LB, TT,
689 and HH. Markov chain Monte Carlo simulations were run by AA. The manuscript was
690 written by JEV with input of all co-authors.

691

692 **References**

693 Anderson, L. G., Jutterström, S., Hjalmarsson, S., Wählström, I., and Semiletov, I.P.:

694 Out-gassing of CO₂ from Siberian Shelf seas by terrestrial organic matter
695 decomposition, *Geophys. Res. Lett.* 36, L20601, doi:10.1029/2009GL040046,
696 2009.

697 Anderson, L.G., Björk, G., Jutterström, S., Pipko, I., Shakhova, N. Semiletov, I. and
698 Wählström, I.: East Siberian Sea, an Arctic region of very high biogeochemical
699 activity, *Biogeosciences*, 8, 1745-1754, doi:10.5194/bg-8-1745-2011, 2011.

700 Andersson, E., Deng, J., Du, K., Zheng, M., Yan, C., Sköld, M., and Gustafsson, Ö.:
701 Regionally-varying combustion sources of the January 2013 severe haze events
702 over Eastern China, *Environ. Sci. Technol.* 49(4), 2038-2043, doi:
703 10.1021/es503855e, 2015.

704 Bird, M. I., Santruckova, H., Arneeth, A., Grigoriev, S., Gleixner, G., Kalaschnikov, Y. N.,
705 Lloyd, J., and Schulze, E.-D.: Soil carbon inventories and carbon-13 on a latitude
706 transect in Siberia, *Tellus*, 54B, 631-641, 2002.

707 Bröder, L., Tesi, T., Salvado, J.A., Semiletov, I.P., Dudarev, O.V., and Gustafsson, Ö.:
708 Fate of terrigenous organic matter across the Laptev Sea from the mouth of the
709 Lena River to the deep sea of the Arctic interior, *Biogeosciences* 13, 5003, 5019,

Deleted: the Russian Government (mega-grant under contract #14.Z50.31.0012 to I. S.),

Deleted: .

713 doi:10.5194/bg-13-5003-2016, 2016b.

714 Bröder, L., Tesi, T., Andersson, A., Eglinton, T.I., Semiletov, I.P., Dudarev, O.V., Roos,
715 P., and Gustafsson, Ö.: Historical records of organic matter supply and
716 degradation status in the East Siberian Sea, *Org. Geochem.* 91, 16-30,
717 doi:10.1016/j.orggeochem.2015.10.008, 2016a.

718 Bosch, C., Andersson, A., Kruså, M., Bandh, C., Hovorkova, I., Klanova, J., Knowles, T.
719 D. J., Pancost, R. D., Evershed, R. P., and Gustafsson, Ö.: Source apportionment of
720 polycyclic aromatic hydrocarbons in central European soils with compound-
721 specific triple isotopes ($\delta^{13}\text{C}$, $\Delta^{14}\text{C}$, and $\delta^2\text{H}$), *Environ. Sci. Technol.* 49(13), 7657-
722 7665, doi:10.1021/acs.est.5b01190, 2015.

723 Bush, R.T., and McInerney, F.A.: Leaf wax n-alkane distributions in and across
724 modern plants: Implications for paleoecology and chemotaxonomy, *Geochim.*
725 *Cosmochim. Ac.* 117, 161-179, 2013.

726 Craig, H.: Isotopic variations in meteoric waters, *Science* 133: 1702-1703, 1961.

727 Dansgaard, W.: Stable isotopes in precipitation, *Tellus*, 16, 436- 438, 1964.

728 Eglinton, G., and Hamilton, R.J.: Leaf epicuticular waxes, *Science* 156, 1322-1335,
729 1967.

730 Gundelwein, A., Mueller-Lupp, T., Sommerkorn, M., Haupt, E. T. K., Pfeiffer, E. M., and
731 Wiechmann, H.: Carbon in tundra soils in the Lake Labaz region of arctic Siberia,
732 *Eur. J. Soil Sci.*, 58, 1164-1174, 2007.

733 Günther, F., Overduin, P.P., Sandakov, A.V., Grosse, G., and Grigoriev, M.N.: Short- and
734 long-term thermo-erosion of ice-rich permafrost coasts in the Laptev Sea region,
735 *Biogeosciences*, 10, 4297-4318, doi:10.5194/bg-10-4297-2013, 2013.

736 Hedges, J.I., and Prahl, F.G.: Early diagenesis: consequences for applications of
737 molecular biomarkers, in *Organic Geochemistry: principles and applications*. Engel,
738 M.H., and Macko, S.A. (ed.). Plenum Press, New York. pp 237-253, 1993.

739 Höfle, S., Rethemeyer, J., Mueller, C. W., and John, C.: Organic matter composition and
740 stabilization in a polygonal tundra soil of the Lena Delta, *Biogeosciences*, 10, 3145-
741 3158, doi:10.5194/bg-10-3145-2013, 2013

742 Hugelius, G. Strauss, J., Zubrzycki, S., Harden, J. W., Schuur, E. A. G., Ping, C.-L.,
743 Schirrmeister, L., Grosse, G., Michaelson, G. J., Koven, C. D., O'Donnell, J. A., Elberling,
744 B., Mishra, U., Camill, P., Yu, Z., Palmtag, J., and Kuhry, P.: Estimated stocks of
745 circumpolar permafrost carbon with quantified uncertainty ranges and identified
746 data gaps, *Biogeosciences* 11, 6573-6593, doi:10.5194/bg-11-6573-2014, 2014.

747 Jasinski, J. P. P., Warner, B. G., Andreev, A. A., Aravena, R., Gilbert, S. E., Zeeb, B. A., Smol,
748 J. P., and Velichko, A. A.: Holocene environmental history of a peatland in the Lena
749 River valley, Siberia, *Can. J. Earth Sci.*, 35, 637-648, 1998.

750 Johnsen, S. J., Dahl-Jensen, D., Gundestrup, N., Steffensen, J. P., Clausen, H. B., Miller,
751 H.: Oxygen isotope and palaeotemperature records from six Greenland ice-core
752 stations: Camp Century, Dye-3, GRIP, GISP2, Renland and NorthGRIP, *J. Quat. Sci.*
753 16, 299-307, doi:10.1002/jqs.622, 2001.

754 Kaiser, C., Meyer, H., Biasi, C., Rusalimova, O., Barsukov, P., and Richter, A.:
755 Conservation of soil organic matter through cryoturbation in arctic soils in
756 Siberia, *J. Geophys. Res.-Biogeosciences*, 112, G2, doi:10.1029/2006JG000258,
757 2007.

758 Karlsson, E. S., Charkin, A., Dudarev, O., Semiletov, I., Vonk, J. E., Sanchez-Garcia, L.,

Deleted: .
Formatted: Font:12 pt, Not Italic
Formatted: Font:12 pt, Not Italic
Formatted: Font:12 pt, Not Italic
Formatted: Font:12 pt, Not Italic
Formatted: p1, Indent: Left: 0 cm, First line: 0 cm, Add space between paragraphs of the same style, Widow/Orphan control, Adjust space between Latin and Asian text, Adjust space between Asian text and numbers
Formatted: Font:+Theme Body (Cambria), 12 pt
Formatted: Font:+Theme Body (Cambria)
Deleted: .

761 Andersson, A., and Gustafsson, O.: Carbon isotopes and lipid biomarker
 762 investigation of sources, transport and degradation of terrestrial organic matter
 763 in the Buor-Khaya Bay, SE Laptev Sea, Biogeosciences 8, 1865-1879,
 764 doi:10.5194/bg-8-1865-2011, 2011.

765 Karlsson, E. S., Gelting, J., Tesi, T., van Dongen, B., Andersson, A., Semiletov, I.,
 766 Charkin, Al., Dudarev, O., and Gustafsson, Ö.: Different sources and degradation
 767 state of dissolved, particulate, and sedimentary organic matter along the Eurasian
 768 Arctic coastal margin, Global Biogeochem. Cycles, 30, 898-919,
 769 doi:10.1002/2015GB005307, 2016.

770 Kotler, E., and Burn, C. R.: Cryostratigraphy of the Klondike “muck” deposits,
 771 westcentral Yukon Territory, Can. J. Earth Sci. 37, 849-861, doi:10.1139/e00-013,
 772 2000.

773 Leaney, F. W., Osmond, C. B., Allison, G. B., and Ziegler, H.: Hydrogen-isotope
 774 composition of leaf water in C-3 and C-4 plants - its relationship to the hydrogen
 775 isotope composition of dry-matter, Planta 164 (2), 215-220, 1985.

776 Meyer, H., Opel, T., Laepple, T., Dereviagin, A.Y., Hoffmann, K., and Werner, M.: Long-
 777 term winter warming trend in the Siberian Arctic during the mid- to late
 778 Holocene, Nat. Geosci. 8, 122-125, doi:10.1038/ngeo2349, 2015.

779 Meyers P. A., Ishiwatari R.: Lacustrine organic geochemistry – an overview of
 780 indicators of organic matter sources and diagenesis in lake sediments, Org.
 781 Geochem. 20, 867-900, doi:10.1016/0146-6380(93)90100-P, 1993.

782 Meyers, P. A.: Preservation of elemental and isotopic source identification of
 783 sedimentary organic matter, Chem. Geol. 114, 289-302, doi:10.1016/0009-
 784 2541(94)90059-0, 1994.

785 Meyers, P. A.: Organic geochemical proxies of paleoceanographic, paleolimnologic
 786 and paleoclimatic processes, Org. Geochem. 27, 213-250, doi:10.1016/S0146-
 787 6380(97)00049-1, 1997.

788 Nott, C. J., Xie, S., Avsejs, L. A., Maddy, D., Chambers, F. M., Evershed, R. P.: *n*-Alkane
 789 distributions in ombrotrophic mires as indicators of vegetation change related to
 790 climatic variation, Org. Geochem. 31, 231-235, doi:10.1016/S0146-
 791 6380(99)00153-9, 2000.

792 Opel, T., Dereviagin, A. Y., Meyer, H., Schirrmeister, L., and Wetterich, S.:
 793 Palaeoclimatic information from stable water isotopes of Holocene ice wedges on
 794 the Dmitrii Laptev Strait, Northeast Siberia, Russia, Permafrost Periglacial
 795 Process., 22, 84-100, 10.1002/ppp.667, 2011.

796 Opel, T., Wetterich, S., Meyer, H., Dereviagin, A.Y., Fuchs, M.C., and Schirrmeister, L.:
 797 Ground-ice stable isotopes and cryostratigraphy reflect late Quaternary
 798 palaeoclimate in the Northeast Siberian Arctic (Oyogos Yar coast, Dmitry Laptev
 799 Strait), Clim. Past Discuss., doi:10.5194/cp-2017-1, 2017.

800 Palmtag J., Hugelius G., Lashchinskiy N., Tamstorf M.P., Richter A., Elberling B. and
 801 Kuhry, P.: Storage, Landscape Distribution, and Burial History of Soil Organic
 802 Matter in Contrasting Areas of Continuous Permafrost, Arctic, Antarctic, and Alpine
 803 Research, 47(1), 71-88, doi: http://dx.doi.org/10.1657/AAAR0014-027, 2015.

804 Polissar, P. J., and Freeman, K. H.: Effects of aridity and vegetation on plant-wax dD in
 805 modern lake sediments, Geochim. Cosmochim. Ac. 74, 5785-5797,
 806 doi:10.1016/j.gca.2010.06.018, 2010.

Deleted: .

Deleted: .

Deleted: .

Formatted: Font:Times New Roman

Deleted: (2015)

- 811 Panova, E., Tesi, T., Pearce, C., Salvado, J. A., Karlsson, E. S., Kruså, M., Semiletov, I. P.,
812 and Ö. Gustafsson: Geochemical compositional differences of the supramicron
813 plankton-dominated fraction in two regimes of the Marginal Ice Zone (MIZ) of the
814 outer East Siberian Arctic Shelf, AGU Fall meeting 2015 abstract, 2015.
- 815 Pautler, B. G., Reichart, G.-J., Sanborn, P. T., Simpson, M. J., Weijers, J. W. H.:
816 Comparison of soil derived tetraether membrane lipid distributions and plantwax
817 dD compositions for reconstruction of Canadian Arctic temperatures,
818 *Palaeogeogr. Palaeoclimatol. Palaeoecol.* 404, 78-88,
819 doi:10.1016/j.palaeo.2014.03.038, 2014
- 820 Porter, T. J., Froese, D. G., Feakins, S. J., Bindeman, I. N., Mahoney, M. E., Pautler, B. G.,
821 Reichart, G.-J., Sanborn, P. T., Simpson, M. J., and Weijers, J. W. H.: Multiple water
822 isotope proxy reconstruction of extremely low last glacial temperatures in
823 Eastern Beringia (Western Arctic), *Quat. Sci. Rev.* 137, 113-125,
824 doi:10.1016/j.quascirev.2016.02.006, 2016.
- 825 Rodionow, A., Flessa, H., Kazansky, O., and Guggenberger, G.: Organic matter
826 composition and potential trace gas production of permafrost soils in the forest
827 tundra in northern Siberia, *Geoderma*, 135, 49-62, 2006.
- 828 Romanovsky, N. N.: *Fundamentals of the cryogenesis of the lithosphere*. University
829 Press, Moscow, pp. 1-336 (in Russian), 1993.
- 830 Sachse, D., Radke, J., and Gleixner, G.: Hydrogen isotope ratios of recent lacustrine
831 sedimentary n-alkanes record modern climate variability, *Geochim. Cosmochim.*
832 *Ac.*, 68, 4877-4889, doi:10.1016/j.gca.2004.06.004, 2004.
- 833 Schuur, E. A. G., McGuire, A. D., Schädel, C., Grosse, G., Harden, J. W., Hayes, D. J.,
834 Hugelius, G., Koven, C. D., Kuhry, P., Lawrence, D. M., Natali, S. M., Olefeldt, D.,
835 Romanovsky, V. E., Schaefer, K., Turetsky, M. R., Treat, C. C., and Vonk, J. E.:
836 Climate change and the permafrost carbon feedback, *Nature*, 250, 171-178,
837 doi:10.1038/nature14338, 2015.
- 838 Schirrmeister, L., Kunitsky, V. V., Grosse, G., Wetterich, S., Meyer, H., Schwamborn, G.,
839 Babiy, O., Derevyagin, A., and Siegert, C.: Sedimentary characteristics and origin of
840 the Late Pleistocene Ice Complex on north-east Siberian Arctic coastal lowlands
841 and islands – A review, *Quatern. Int.* 241, 3-25, doi:10.1016/j.quaint.2010.04.004,
842 2011.
- 843 Semiletov I.P., Pipko I.I., Shakhova N.E., Dudarev O.V., Pugach S.P., Charkin A.N., McRoy
844 C.P., Kosmach D., and Gustafsson, Ö: Carbon transport by the Lena River from its
845 headwaters to the Arctic Ocean, with emphasis on fluvial input of terrestrial
846 particulate organic carbon vs. carbon transport by coastal erosion, *Biogeosciences*,
847 8, 2407-2426, 2011.
- 848 Semiletov I.P., Shakhova N. E., Sergienko V.I., Pipko I.I., and O. Dudarev: On Carbon
849 Transport and Fate in the East Siberian Arctic Land-Shelf-Atmosphere System,
850 *Environment Res. Lett.*, 7, doi:10.1088/1748-9326/7/1/015201, 2012.
- 851 Semiletov, I.P., Shakhova, N.E., Pipko, I.I., Pugach, S.P., Charkin, A.N., Dudarev, O.V.,
852 Kosmach, D.A., and S. Nishino (2013). Space-time dynamics of carbon and
853 environmental parameters related to carbon dioxide emissions in the Buor-Khaya
854 Bay of the Laptev Sea, *Biogeosciences*, 10, 5977-5996, doi:10.5194/bg-10-5977-
855 2013

857 Semiletov I., Pipko I., Gustafsson O., Anderson L., Sergienko V., Pugach S., Dudarev O.,
858 Charkin A., Broder L., Andersson A., Spivak E., and N. Shakhova (2016),
859 Acidification of the East Siberian Arctic Shelf waters through addition of
860 freshwater and terrestrial carbon, *Nature Geoscience*, doi:10.1038/NEGO 2695,
861 2016.

862 Semiletov I.P., Pipko, I.I., Pivovarov, N.Y., Popov, V. V., Zimov, S. A., Voropaev, Y. V.,
863 and S.P. Davydov: Atmospheric carbon emissions from northern lakes: a factor of
864 global significance, *Atmospheric Environment*, 30, 1657-1671, 1996a.

865 Semiletov I.P., Pivovarov, N.Y., Pipko, I. I., Gukov, A. Y., Volkova, T. I., Sharp, J. P.,
866 Shcherbakov, Y. S., and K. P. Fedorov: Dynamics of dissolved CH₄ and CO₂ in the
867 Lena River Delta and Laptev Sea. *Transactions (Doklady) of the Russian Academy
868 of Sciences*, 350 (3), 401-404 (translated into English), 1996b.

869 Semiletov, I.P.: Destruction of the coastal permafrost ground as an important factor
870 in biogeochemistry of the Arctic Shelf waters, *Trans. (Doklady) Russian Acad. Sci.*,
871 368, 679-682 (translated into English), 1999.

872 Sessions, A.L., Burgoyne, T.W., and Hayes, J.M.: Determination of the H3 factor in
873 hydrogen isotope ratio mass spectrometry, *Anal. Chem.* 73(2), 200-207, 2001.

874 Siewert, M.B., Hanisch, J., Weiss, N., Kuhry, P., Maximov, T.C., Hugelius, G.: Comparing
875 carbon storage of Siberian tundra and taiga permafrost ecosystems at very high
876 spatial resolution. *J. Geophys. Res.: Biogeosciences*, 120,
877 doi:10.1002/2015JG002999, 2015.

878 Siewert, M.B., Hugelius, G., Heim, B., Faucherre, S.: Landscape controls and vertical
879 variability of soil organic carbon storage in permafrost-affected soils of the Lena
880 River Delta. *Catena*, 147, 725-741. doi:10.1016/j.catena.2016.07.048, 2016.

881 Soil Survey Staff. *Keys to Soil Taxonomy*, 12th ed., U.S. Department of Agriculture &
882 Natural Resources Conservation Service, Washington, D. C., 2014.

883 Sessions, A. L., Burgoyne, T.W., Schimmelmann, A., and Hayes, J. M.: Fractionation of
884 hydrogen isotopes in lipid biosynthesis, *Org. Geochem.*, 30, 1193-1200,
885 doi:10.1016/S0146-6380(99)00094-7, 1999.

886 Sessions, A.L., Sylva, S.P., Summons, R.E., and Hayers, J.M.: Isotopic exchange of
887 carbon-bound hydrogen over geologic timescales, *Geochim. Cosmochim. Ac.* 68,
888 1545-1559, doi:10.1016/j.gca.2003.06.004, 2004.

889 Shakhova, N. and I. Semiletov: Methane release and coastal environment in the East
890 Siberian Arctic shelf, *Journal of Marine Systems*, 66 (1-4), 227-243, 2007.

891 Shakhova, N., Semiletov I., Leifer, I., , Sergienko, V., Salyuk, A., Kosmach, D., Chernikh
892 D., Stubbs Ch., Nicolsky D., Tumskoy V., and O. Gustafsson: Ebullition and storm-
893 induced methane release from the East Siberian Arctic Shelf, *Nature Geoscience*
894 7-1, 64-70, doi: 10.1038/NGEO2007, 2014.

895 Shakhova N., I. Semiletov, V. Sergienko, L. Lobkovsky, V. Yusupov, A. Salyuk, A.
896 Salomatin, D. Chernykh, D. Kosmach, G. Panteleev, D. Nicolsky, V. Samarkin, S.
897 Joye, A. Charkin, O. Dudarev, A. Meluzov, and Ö. Gustafsson: The East Siberian
898 Arctic Shelf: towards further assessment of permafrost-related methane fluxes and
899 role of sea ice. *Phil. Trans. R. Soc. A*, vol. 373: 20140451.
900 doi:10.1098/rsta.2014.0451, 2015.

901 Shanahan, T.M., HUGHEN, K.A., AMPLE, L., SAUER, P.E., and FORNACE, K.: Environmental

Deleted: urnal of

Deleted: ical

Deleted: earch

Deleted: (2014),

Deleted: .

907 controls on the 2H/1H values of terrestrial leaf waxes in the eastern Canadian
908 Arctic, *Geochim. Cosmochim. Ac.* 119, 286-301, doi:10.1016/j.gca.2013.05.032,
909 2013.

910 Shiklomanov, N. I., Streletskiy, D. A., Little, J. D., and Nelson, F. E.: Isotropic thaw
911 subsidence in undisturbed permafrost landscapes, *Geophys. Res. Lett.* 40, 6356-
912 6361, doi:10.1002/2013GL058295, 2013.

913 Smith, F.A., and Freeman, K.H.: Influence of physiology and climate on dD of leaf wax
914 n-alkanes from C3 and C4 grasses, *Geochim. Cosmochim. Ac.* 70, 1172-1187,
915 doi:10.1016/j.gca.2005.11.006, 2006.

916 Strauss, J., Schirrmeister, L., Grosse, G., Wetterich, S., Ulrich, M., Herzschuh, U., and
917 Hubberten, H.-W.: The deep permafrost carbon pool of the Yedoma region in
918 Siberia and Alaska. *Geophys. Res. Lett.* 40, 6165-6170,
919 doi:10.1002/2013GL058088, 2013.

920 Tesi, T., I. Semiletov, G. Hugelius, O. Dudarev, P. Kuhry, and Gustafsson, Ö.:
921 Composition and fate of terrigenous organic matter along the Arctic land-ocean
922 continuum in East Siberia: insights from biomarkers and carbon isotopes,
923 *Geochim. Cosmochim. Acta*, 133, 235-256, 2014.

924 Tesi, T., Semiletov, I., Dudarev, O., Andersson, A., and Gustafsson, Ö.: Matrix
925 association effects on hydrodynamic sorting and degradation of terrestrial organic
926 matter during cross-shelf transport in the Laptev and East Siberian shelf seas, *J.*
927 *Geophys. Res.-Biogeosciences*, 121, 731-752, doi:10.1002/2015JG003067, 2016a.

928 Tesi, T., Muschitiello, F., Smittenberg, R. H., Jakobsson, M., Vonk, J. E., Hill, P.,
929 Andersson, A., Kirchner, N., Noormets, R., Dudarev, O., Semiletov, I., and Gustafsson,
930 Ö.: Massive remobilization of permafrost carbon during post-glacial warming, in
931 review at *Nature Communications*, 2016b.

932 Vonk, J. E., van Dongen, B. E., and Gustafsson, Ö.: Selective preservation of old organic
933 carbon fluvially released from sub-arctic soils, *Geophys. Res. Lett.* 37, L11605,
934 2010

935 Vonk, J. E., Sanchéz-García, L., van Dongen, B. E., Alling, V., Kosmach, D., Charkin, A.,
936 Semiletov, I. P., Dudarev, O. V., Shakhova, N., Roos, P., Eglinton, T. I., Andersson, A.,
937 and Gustafsson, Ö.: Activation of old carbon by erosion of coastal and subsea
938 permafrost in Arctic Siberia, *Nature*, 489, 137-140, doi:10.1038/nature11392,
939 2012.

940 Vonk, J. E., and Gustafsson, Ö.: Permafrost-carbon complexities, *Nat. Geosci.* 6, 675-
941 676, doi:10.1038/ngeo1937, 2013.

942 Vonk, J. E., Mann, P. J., Davydov, S., Davydova, A., Spencer, R. G. M., Schade, J.,
943 Sobczak, W. V., Zimov, N., Zimov, S., Bulygina, E., Eglinton, T. I., and Holmes, R. M.:
944 High biolability of ancient permafrost carbon upon thaw, *Geophys. Res. Lett.*, 40,
945 2689-2693, doi:10.1002/grl.50348, 2013.

946 Vonk, J. E., Semiletov, I. P., Dudarev, O. V., Eglinton, T. I., Andersson, A., Shakhova, N.,
947 Charkin, A., Heim, B., and Gustafsson, Ö.: Preferential burial of permafrost-derived
948 organic carbon in Siberian-Arctic shelf waters, *J. Geophys. Res. Oceans* 119, 8410-
949 8421, doi:10.1002/2014JC010261, 2014.

950 Vonk, J. E., Tank, S. E., Bowden, W. B., Laurion, I., Vincent, W. F., Alekseychik, P., Amyot,
951 M., Billet, M. F., Canario, J., Cory, R. M., Deshpande, B. N., Helbig, M., Jammet, M.,
952 Karlsson, J., Larouche, J., MacMillan, G., Rautio, M., Walter Anthony, K. M., and

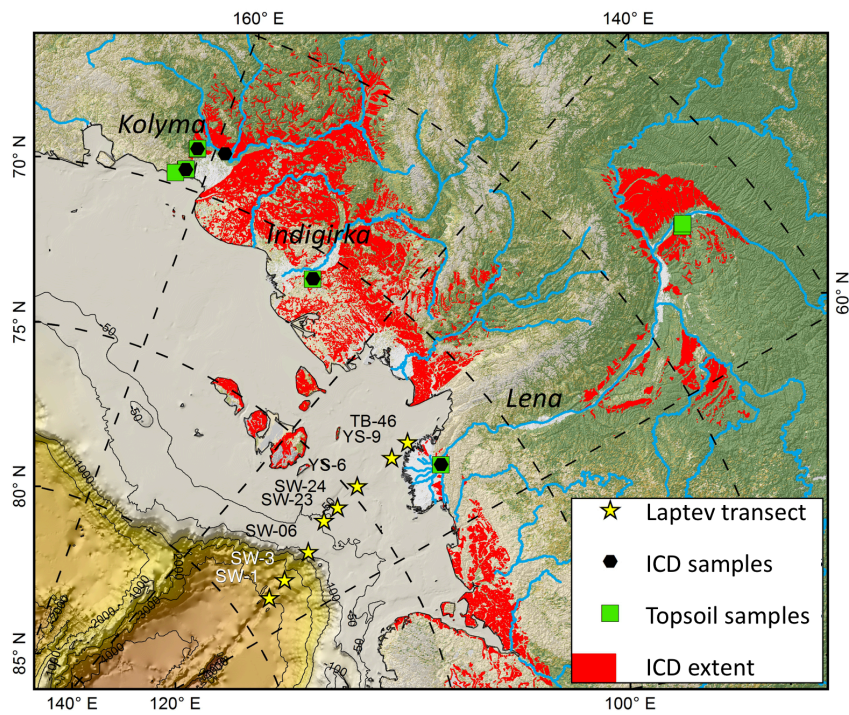
- 953 Wickland, K. P.: Effects of permafrost thaw on Arctic aquatic ecosystems,
 954 Biogeosciences 12, 7129-7167, doi:10.5194/bg-12-7129-2015, 2015.
- 955 Walvoord, M. A., Voss, C. I., and Wellman, T. P.: Influence of permafrost distribution
 956 on groundwater flow in the context of climate-driven permafrost thaw: Example
 957 from Yukon Flats Basin, Alaska, United States, Water Resour. Res. 48, W07524,
 958 doi:10.1029/2011WR011595, 2012.
- 959 Weiss N, Blok D, Elberling B, Hugelius G, Jørgensen CJ, Siewert MB, Kuhry P:
 960 Thermokarst dynamics and soil organic matter characteristics controlling initial
 961 carbon release from permafrost soils in the Siberian Yedoma region. Sedimentary
 962 Geology, <http://dx.doi.org/10.1016/j.sedgeo.2015.12.004>, 2015.
- 963 [Wetterich, S., Tumskov, V., Rudaya, N., Kuznetsov, V., Maksimov, F., Opel, T., Meyer,](#)
 964 [H., Andreev, A. A., and Schirrmeister, L.: Ice Complex permafrost of MIS5 age in](#)
 965 [the Dmitry Laptev Strait coastal region \(East Siberian Arctic\), Quaternary Science](#)
 966 [Reviews, 147, 298-311, 10.1016/j.quascirev.2015.11.016, 2016.](#)
- 967 Wiesenberg, G., Schwark, L., ~~and~~ Schmidt, M.: Improved automated extraction and
 968 separation procedure for soil lipid analyses. European Journal of Soil Science 55,
 969 349-356, 2014.
- 970 Wilkie, K.M.K., Chaplgin, B., Meyer, H., Burns, S., Petsch, S., and Brigham-Grette, J.:
 971 Modern isotope hydrology and controls on dD of plant leaf waxes at Lake
 972 El'gygytgyn, NE Russia, Clim. Past 9, 335-352, doi:10.5194/cp-9-335-2013, 2013.
- 973 Winterfeld, M., Lepple, T., and Mollenhauer, G.: Characterization of particulate
 974 organic matter in the Lena River delta and adjacent nearshore zone, NE Siberia –
 975 Part I: Radiocarbon inventories, Biogeosciences, 12, 3769-3788, doi:10.5194/bg-
 976 12-3769-2015, 2015.
- 977 Yang, H., Liu, W., Leng, Q., Hren, M.T., and Pagani, M.: Variation in n-alkane dD values
 978 from terrestrial plants at high latitude: implications for paleoclimate
 979 reconstruction, Org. Geochem. 42, 283-288,
 980 doi:10.1016/j.orggeochem.2011.01.006, 2011.
- 981 Zech, R., Huang, Y., Zech, M., Tarozo, R., and W. Zech: High carbon sequestration in
 982 Siberian permafrost loess-paleosols during glacials, Clim. Past, 7, 501-509,
 983 doi:10.5194/cp-7-501-2011, 2011.
- 984 Zimov, S.A., Semiletov, I. P. Daviodov, S. P., Voropaev, Y. V., Prosyannikov, S. F., Wong,
 985 C. S., and Y.-H. Chan: Wintertime CO₂ emission from soils of Northeastern Siberia.
 986 Arctic, 46, 197-204, 1993.
- 987

Deleted: ,

Deleted: 2004.

Deleted: .

991 **Figure 1**
992 Map of coastal northeast Siberia showing the extent of ice complex permafrost (ICD; red)
993 overlaid with the location of ice complex (n=9; black diamonds) and topsoil samples
994 (n=9; green squares). The shelf-slope Laptev Sea transect is shown with yellow stars.
995
996



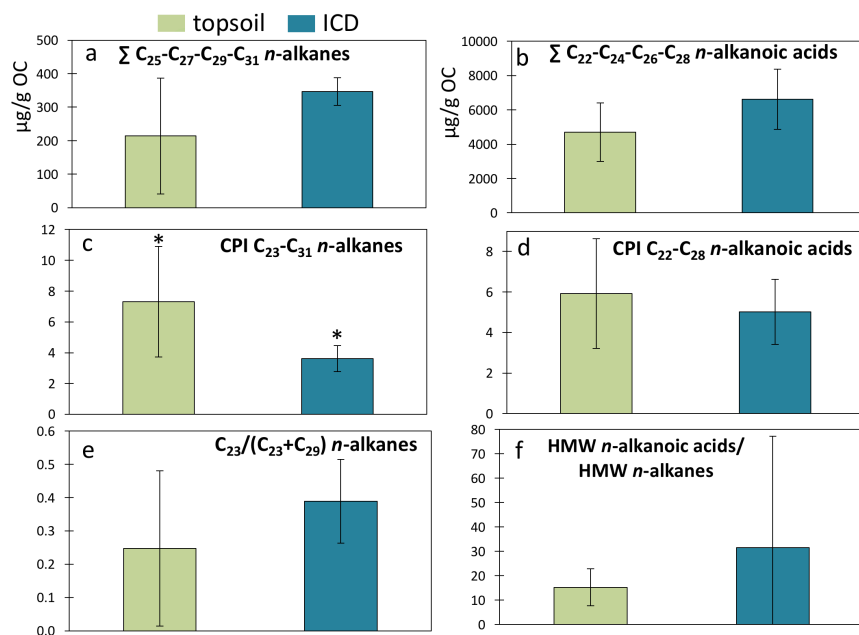
997
998

999
1000
1001
1002
1003
1004
1005
1006
1007
1008
1009
1010

Figure 2

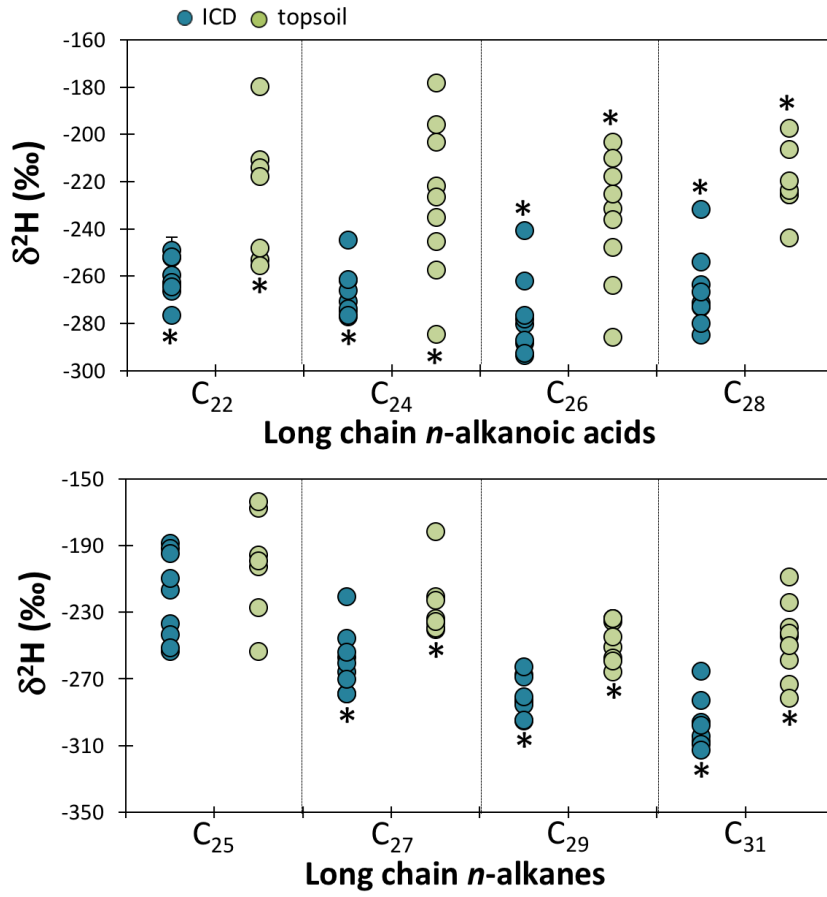
Molecular concentrations and ratios of topsoil Holocene permafrost (green; $n=9$) and deeper Pleistocene permafrost (blue; $n=9$) samples, with (a) the sum of odd n -alkanes C_{25} - C_{31} , (b) the sum of even n -alkanoic acids C_{22} - C_{28} , (c) the Carbon Preference Index (CPI) for n -alkanes C_{23} - C_{31} , (d), the CPI for n -alkanoic acids C_{22} - C_{28} , (e) the ratio of C_{23} over $C_{23}+C_{29}$ n -alkanes, and (f) the sum of high-molecular weight (HMW) n -alkanoic acids over HMW n -alkanes. The CPI is calculated as $CPI_{i-n} = \frac{1}{2} \frac{\sum (X_i+X_{i+2}+\dots+X_n)}{\sum (X_{i-1}+X_{i+1}+\dots+X_{n-1}) + \frac{1}{2} \sum (X_i+X_{i+2}+\dots+X_n)} / \frac{\sum (X_{i+1}+X_{i+3}+\dots+X_{n+1})}{\sum (X_{i-1}+X_{i+1}+\dots+X_{n-1})}$, where X is concentration. Stars indicate that the two compared values are statistically significant (95% confidence). Note that panel a and b are reported as median with IQR (interquartile range) and the other panels are reported as average \pm standard deviation.

Deleted: 5
Deleted: 5
Deleted: ±



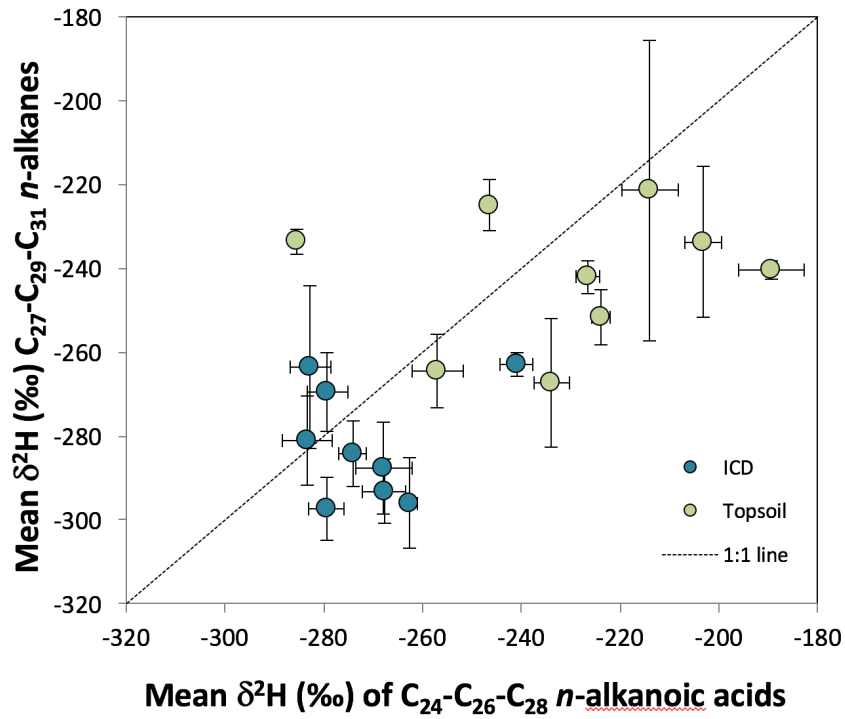
1011
1012

1016 **Figure 3**
 1017 Molecular isotopic signature against chain length of long chain *n*-alkanoic acids (top) and
 1018 *n*-alkanes (bottom) for Holocene topsoil samples (green) and Pleistocene ice complex
 1019 samples (ICD; blue). Stars indicate that the two compared values are statistically
 1020 significant (95% confidence). Standard deviations are represented as vertical bars, and
 1021 are smaller than the sample circles when not visible.
 1022



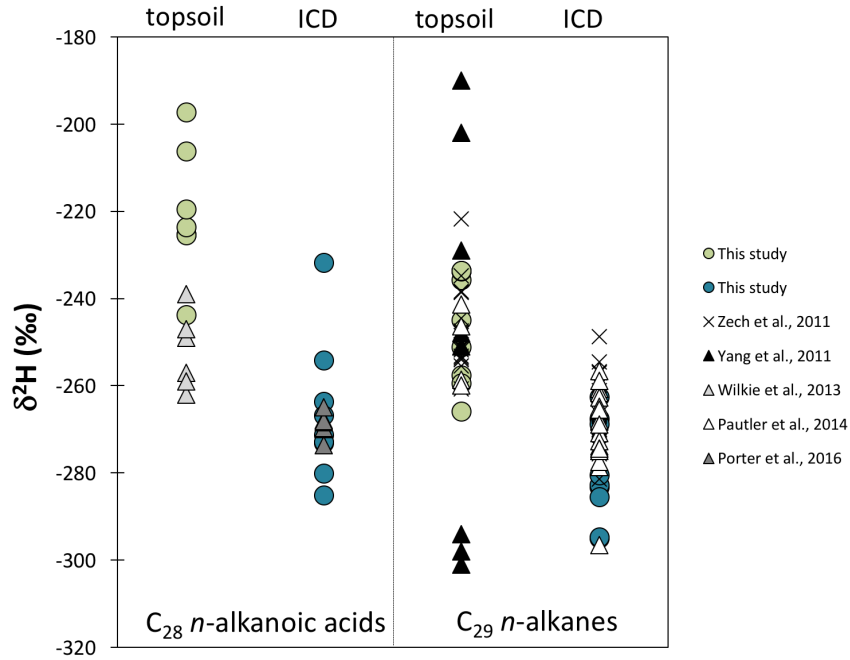
1023
 1024
 1025
 1026
 1027

1028 **Figure 4**
1029 Concentration-weighted mean $\delta^2\text{H}$ values of $\text{C}_{27}\text{-C}_{29}\text{-C}_{31}$ *n*-alkanes plotted against
1030 concentration-weighted mean $\delta^2\text{H}$ values of $\text{C}_{24}\text{-C}_{26}\text{-C}_{28}$ *n*-alkanoic acids to illustrate the
1031 fractionation differences between these two leaf wax markers. Dashed line indicates an
1032 identical fractionation.
1033



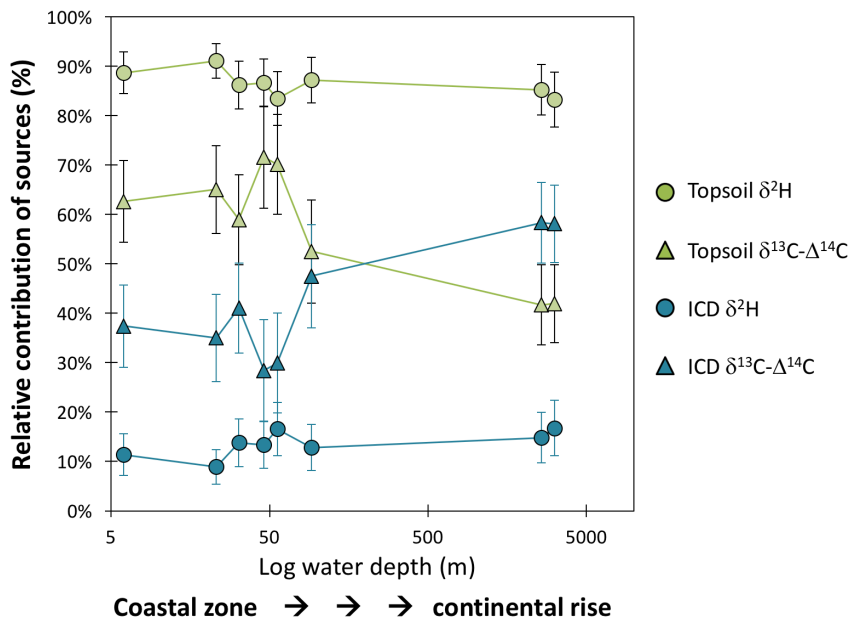
1034
1035

1036 **Figure 5**
 1037 Comparison of $\delta^2\text{H}$ values of C_{28} *n*-alkanoic acid (left) and C_{29} *n*-alkane (right) in
 1038 modern (Topsoil-PF; green circles) and ICD-PF for this study (blue circles) and
 1039 available literature, with crosses from Zech et al. (2011; glacial and interglacial
 1040 paleosoils from permafrost bluff exposure at Tumara River northeast Siberia), black
 1041 triangles from Yang et al. (2011; C3 plants and trees from Canada and Alaska), light
 1042 grey triangles from Wilkie et al. (2013; C3 plants from the El'gygytgyn lake basin,
 1043 Siberia), white triangles from Pautler et al. (2014; modern and paleosoils from the
 1044 Yukon territory, Canada) and dark grey triangles from Porter et al. (2016; muck
 1045 deposits from the Yukon territory, Canada).
 1046



1047
 1048
 1049
 1050

1051 **Figure 6**
 1052 Contribution of OC from Topsoil-PF (green) and ICD-PF (blue) sources to surface
 1053 sediments along a shelf-slope transect in the Laptev Sea (see also Bröder et al., 2016b for
 1054 further transect information), calculated with a $\delta^{13}\text{C}$ - $\Delta^{14}\text{C}$ (triangles) and leaf wax $\delta^2\text{H}$
 1055 mixing model (circles). Stations are plotted against log water depth (m; see also Table 6)
 1056 following the transect order from the coastal, nearshore, zone in the South (furthest left;
 1057 TB-46, 6 m depth) towards the continental rise in the North (furthest right; SW-01, 3146
 1058 m depth). Topsoil $\Delta^{14}\text{C}$ end-member values are corrected for cross-shelf transport time
 1059 (see section 4.2).
 1060



1061

Table 1

Site characteristics and geochemical properties of eight topsoil and eight ice complex deposit samples. A table with more detailed sample descriptions can be found in Supplementary Table 1. *n.a.* indicates "not available".

Sample code	Sample ID	Current vegetation	Watershed Description	Lat	Lon	TOC	δ ¹³ C		¹⁴ C yrs	Formatted Table	
							°N	°E		%	‰
Topsoil (modern vegetation and O-horizon samples)											
TS-1	KU EXP 1-1, 0-16 cm	Tundra	Lena	Surface O-horizon; 0-16 cm	72.34	126.29	11	-27.0	n.a.	0.40	27.5
TS-2	CH YED2, 0-4 cm	Tundra	Kolyma	Surface O-A horizon; 0-4 cm	69.46	161.79	17	-28.4	n.a.	0.64	26.5
TS-3	SP T3-3B,	Alas grassland	Lena	Alas soil (Mollisol), mix of O and A horizon	62.32	129.50	15	-27.9	n.a.	1.40	10.7
TS-4	SP T2-7,	Larch taiga	Lena	Taiga soil (turbel), mix of O and A horizon	62.25	129.62	13	-28.4	n.a.	0.45	28.0
TS-5	KY T2-3,	Tussock tundra	Indigirka	Tundra soil (turbel), O-horizon	70.83	147.48	29	-28.5	n.a.	1.56	18.7
TS-6	CH T2-1,	Tussock tundra	Kolyma	Tundra soil (turbel), mix of O, Ojj and Ajj horizons	69.44	161.77	21	-26.4	n.a.	0.57	36.7
TS-7	CH YED3, 0-10 cm	Larch taiga	Kolyma	Surface O-hor; 0-10 cm	68.77	161.41	39	-29.6	n.a.	1.29	30.7
TS-8G^a	CH Medv grass ^a	Grass tundra	Kolyma	Vegetation	69.64	162.54	41	-25.2	n.a.	Formatted: Superscript	
TS-9G^a	CH Y4 grass ^a	Larch taiga	Kolyma	Vegetation	68.74	161.41	40	-28.5	n.a.	Formatted: Superscript	
Mean values						25	-27.8	1.1	24.8		
Ice complex deposits											
ICD-1	KU EXP 1-3, 212-216 cm	Tundra	Lena	Very deep undisturbed yedoma ca. 10 m below surface	72.34	126.29	1.3	-27.5	n.a.	0.08	15.7
ICD-2	CH YED1, 300-305 cm	Tussock tundra	Kolyma	Deep undisturbed yedoma ca. 3 m below surface	69.47	161.77	1.4	-26.3	n.a.	0.14	10.2
ICD-3	CH YED2, 300-305 cm	Tussock tundra	Kolyma	Deep undisturbed yedoma ca. 3 m below surface	69.46	161.79	2.3	-25.8	n.a.	0.27	8.6
ICD-4	CH YED3, 520-525 cm	Larch taiga	Kolyma	Deep undisturbed yedoma ca. 5 m below surface	68.77	161.41	1.4	-25.5	n.a.	0.15	9.7
ICD-5	KY EXP1, 0-5 cm	Tussock tundra	Indigirka	Undisturbed yedoma ca. 2 m below surface	70.83	147.44	1.5	-25.5	27920 ±210	0.18	8.5

<u>ICD-6</u>	KY EXP2, 110-115 cm	Tussock tundra	Indigirka	Deep undisturbed yedoma ca. 4.5 m below surface	70.83	147.44	1.6	-25.6	<u>17270</u>	0.19	8.6
									<u>±80</u>		
<u>ICD-7</u>	KY EXP3, 185-190 cm	Tussock tundra	Indigirka	Undisturbed yedoma ca. 2 m below surface	70.83	147.49	1.5	-25.2	<u>n.a.</u>	0.17	8.5
<u>ICD-8</u>	CH DY-3A	Larch taiga	Kolyma	Particulate matter from thaw streams	68.63	159.15	1.5 ^b	-25.2 ^b	<u>19370</u>	-	-
									<u>±70</u>		
<u>ICD-9</u>	CH DY-4A	Larch taiga	Kolyma	Particulate matter from thaw streams	68.63	159.15	1.4 ^b	-25.1 ^b	<u>28040</u>	-	-
									<u>±140</u>		
	Mean values						1.6	-25.7		0.2	10.0

a vegetation/grass samples, labelled with "G"

b data from Vonk et al., 2013

Table 2

Long-chain *n*-alkane concentrations (in µg/gOC) of topsoil Holocene samples (modern vegetation/O-horizon) and Pleistocene ice complex samples.

	C21	C22	C23	C24	C25	C26	C27	C28	C29	C30	C31	C32	C33
µg/g OC													
Topsoil (modern vegetation and O-horizon samples)													
<u>TS-1</u>	44	88	96	45	41	10	45	4.4	27	2.5	36	1.5	7.2
<u>TS-2</u>	24	15	21	12	40	10	160	10	150	6.5	150	3.5	17
<u>TS-3</u>	2.5	2.4	5.9	2.6	13	4.7	42	16	74	4.7	85	2.7	24
<u>TS-4</u>	19	3.3	7.1	2.7	27	4.5	47	6.7	98	9.1	150	5.7	38
<u>TS-5</u>	35	8.4	26	9.9	38	13	91	18	180	14	230	8.1	43
<u>TS-6</u>	14	5.1	16	5.7	19	4.0	26	3.7	48	5.0	120	4.0	32
<u>TS-7</u>	46	12	18	8.8	22	16	61	27	220	23	340	12	48
<u>TS-8G</u>	4.1	1.7	18	10	61	16	47	13	30	5.3	10	1.1	1.1
<u>TS-9G</u>	4.7	2.6	18	15	45	21	50	16	31	6.8	9.8	1.5	2.6
Ice complex deposits													
<u>JCD-1</u>	57	79	100	49	82	23	170	16	137	8.5	140	4.4	25
<u>JCD-2</u>	55	89	100	70	70	27	75	20	130	12	120	5.3	28
<u>JCD-3</u>	40	64	74	31	54	15	79	22	110	10	160	4.8	32
<u>JCD-4</u>	60	93	98	47	55	20	84	22	140	12	150	6.0	39
<u>JCD-5</u>	46	79	86	56	49	20	55	13	75	7.0	100	4.7	38
<u>JCD-6</u>	41	73	87	68	62	29	65	20	98	11	120	4.9	27
<u>JCD-7</u>	50	83	83	43	41	16	65	17	100	8.3	120	4.5	42
<u>JCD-8</u>	4.2	7.3	23	30	55	42	82	38	100	18	110	5.0	21
<u>JCD-9</u>	6.2	6.2	16	11	29	15	51	20	79	9.3	85	4.1	23

Deleted: KU EXP 1-1, 0-16 cm**Deleted:** CH YED2, 0-4 cm**Deleted:** SP T3-3B**Deleted:** SP T2-7**Deleted:** KY T2-3**Deleted:** CH T2-1**Deleted:** CH YED3, 0-10 cm**Deleted:** CH Medv grass**Deleted:** CH Y4 grass**Deleted:** KU EXP 1-3, 212-216 cm**Deleted:** CH YED1, 300-305 cm**Deleted:** CH YED2, 300-305 cm**Deleted:** CH YED3, 520-525 cm**Deleted:** KY EXP1, 0-5 cm**Deleted:** KY EXP2, 110-115 cm**Deleted:** KY EXP3, 185-200 cm**Deleted:** CH DY-3A**Deleted:** CH DY-4A

Table 3

Long-chain *n*-alkanoic acids concentrations (in µg/gOC) of topsoil Holocene samples (modern vegetation/O-horizon) and Pleistocene ice complex samples.

	C16	C18	C20	C21	C22	C23	C24	C25	C26	C27	C28	C29	C30	
	µg/gOC													
Topsoil (modern vegetation and O-horizon samples)														
TS-1	511	220	176	80.5	539	311	1100	4.95	684	90.5	350	32.8	58.1	Deleted: KU EXP 1-1, 0-16 cm
TS-2	1740	664	673	235	1380	496	1390	543	1740	409	1580	113	305	Deleted: CH YED2, 0-4 cm
TS-3	664	296	480	116	1020	504	1710	415	1550	250	1060	132	456	Deleted: SP T3-3B
TS-4	1140	408	665	235	1400	431	1410	425	1250	242	651	143	455	Deleted: SP T2-7
TS-5	513	343	530	133	1140	359	1410	1.58	896	119	494	67.8	224	Deleted: KY T2-3
TS-6	1080	537	418	236	1420	790	2670	2.82	1570	127	657	46.6	174	Deleted: CH T2-1
TS-7	1420	352	538	281	1850	722	2010	651	1790	642	1580	730	1971	Deleted: CH YED3, 0-10 cm
TS-8G	3640	855	691	44.1	609	63.5	156	26.0	224	0.122	99.3	9.91	28.1	Deleted: CH Medv grass
TS-9G	4600	887	966	53.6	815	66.7	261	28.6	232	11.5	124	8.10	30.2	Deleted: CH Y4 grass
Ice complex deposits														
ICD-1	1750	1600	4560	1460	9460	2300	8930	2020	5830	1030	3660	293	635	Deleted: KU EXP 1-3, 212-216 cm
ICD-2	10400	4030	5800	2410	17100	7270	18600	6610	16600	5860	14800	6810	18700	Deleted: CH YED1, 300-305 cm
ICD-3	665	554	892	263	2070	1060	3070	646	2340	272	1310	133	532	Deleted: CH YED2, 300-305 cm
ICD-4	1400	769	1030	252	2040	910	3120	644	2440	266	1160	124	432	Deleted: CH YED3, 520-525 cm
ICD-5	426	304	447	126	1220	511	1970	70.4	1390	133	712	60.7	233	Deleted: KY EXP1, 0-5 cm
ICD-6	722	539	583	153	1370	606	2270	457	1970	181	1030	86.4	333	Deleted: KY EXP2, 110-115 cm
ICD-7	446	313	543	158	1330	562	2350	401	1370	154	743	63.1	230	Deleted: KY EXP3, 185-200 cm
ICD-8	920	402	895	108	1070	294	1180	184	799	70.3	331	34.4	100	Deleted: CH DY-3A
ICD-9	327	200	559	74	803	229	1010	2.17	718	64.9	334	28.7	104	Deleted: CH DY-4A

Table 4

Sum of most abundant long-chain *n*-alkanoic acids and *n*-alkanes (concentrations in $\mu\text{g/gOC}$), and characteristic ratios of *n*-alkanoic acids and *n*-alkanes of topsoil Holocene (modern vegetation/O-horizon) and Pleistocene ice complex samples.

	<i>n</i> -alkanoic acids			HMW acids/ HMW alkanes ^a	<i>n</i> -alkanes			$\frac{C_{23}}{C_{23}+C_{25}}$ ^c	$\frac{C_{25}}{C_{25}+C_{29}}$	Formatted Table
	Σ HMW ^a (>C ₂₂) $\mu\text{g/gOC}$	Σ C ₂₂ -C ₂₈ (even) $\mu\text{g/gOC}$	CPI ^b		Σ HMW ^a (>C ₂₁) $\mu\text{g/gOC}$	Σ C ₂₅ -C ₃₁ (odd) $\mu\text{g/gOC}$	CPI ^c			
Topsoil (modern vegetation and O-horizon samples)										
TS-1 _v	3167	2670	5.8	7.1	447	148	2.7	0.78	0.60	Deleted: KU EXP 1-1, 0-16 cm
TS-2 _v	7958	6090	3.8	13	612	494	11	0.12	0.21	Deleted: CH YED2, 0-4 cm
TS-3 _v	7095	5340	4.1	25	280	214	7.2	0.07	0.15	Deleted: SP T3-3B
TS-4 _v	6397	4700	3.7	15	418	323	12	0.07	0.24	Deleted: SP T3-3B
TS-5 _v	4715	3940	6.8	6.6	717	543	9.1	0.12	0.17	Formatted Table
TS-6 _v	7454	6310	6.0	25	300	211	9.9	0.25	0.28	Deleted: SP T2-7
TS-7 _v	11950	7230	2.9	14	857	647	7.8	0.08	0.09	Deleted: KY T2-3
TS-8 _{Gv}	1216	1090	9.5	5.6	217	148	3.7	0.37	0.67	Deleted: KY T2-3
TS-9 _{Gv}	1577	1430	11	7.1	223	135	2.5	0.36	0.59	Deleted: CH T2-1
Mean±stdev	5726±3431	4310±2190	5.9	13	452±230	318±195	7.3	0.25	0.33	Deleted: CH YED3, 0-10 cm
Median and IQR	6397 ⁷⁴⁵⁴ ₃₁₆₇	4700 ⁶⁰⁹⁰ ₆₀₉₂	2.7	7.6	418 ⁶²¹ ₂₈₀	214 ⁴⁹⁴ ₁₄₈	3.6	0.23	0.22	Deleted: CH Medv grass
Ice complex deposits										
ICD-1 _v	34854	27883	4.1	39	893	530	4.9	0.43	0.38	Deleted: CH Y4 grass
ICD-2 _v	112356	67078	2.8	140	806	398	3.0	0.44	0.35	Deleted: Mean (median)
ICD-3 _v	11430	8791	4.1	16	698	405	4.6	0.40	0.33	Deleted: Mean (median) ... [1]
ICD-4 _v	11145	8768	4.4	14	825	428	3.8	0.42	0.29	Deleted: KU EXP 1-3, 212-216 cm
ICD-5 _v	6293	5285	6.5	10	630	280	2.9	0.54	0.40	Deleted: CH YED1, 300-305 cm
ICD-6 _v	8293	6629	4.9	12	708	347	2.7	0.47	0.39	Deleted: CH YED2, 300-305 cm
ICD-7 _v	7196	5787	4.7	11	671	323	3.5	0.45	0.29	Deleted: CH YED3, 520-525 cm
ICD-8 _v	4063	3380	5.5	7.6	533	344	2.7	0.19	0.35	Deleted: CH YED3, 520-525 cm
ICD-9 _v	3295	2867	8.3	9.3	355	244	4.3	0.17	0.27	Deleted: KY EXP1, 0-5 cm
Mean±stdev	22103±35150	15160±20800	5.0	29	680±163	367±85	3.6	0.39	0.34	Deleted: KY EXP2, 110-115 cm
Median and IQR	8290 ¹¹⁴³⁰ ₆₂₉₀	6630 ⁸⁷⁹⁰ ₅₂₈₅	1.6	43	698 ⁸⁰⁶ ₆₃₀	347 ⁴⁰⁵ ₃₂₃	0.8	0.13	0.05	Deleted: KY EXP3, 185-200 cm
										Deleted: CH DY-3A
										Deleted: CH DY-4A
										Deleted: Mean ... [2]

a HMW; high-molecular weight

b CPI; carbon preference index for chain lengths C₂₂-C₂₈, for calculation see caption of Fig. 2.

c CPI; carbon preference index for chain lengths C₂₃-C₃₁, for calculation see caption of Fig. 2.

Table 5

$\delta^2\text{H}$ signatures (in ‰) of *n*-alkanoic acids and *n*-alkanes of topsoil Holocene (modern vegetation/O-horizon) and Pleistocene ice complex samples.

	<i>n</i> -alkanoic acids							<i>n</i> -alkanes			
	C16	C18	C20	C22	C24	C26	C28	C25	C27	C29	C31
Topsoil (modern vegetation and O-horizon samples)											
TS-1	-162	-180		-119	-178	-203	-197	-168	-240	-236	-244
TS-2	-188	-192		-211	-222	-232	-225	-196	-237	-251	-239
TS-3				-126	-203	-218	-225		-125	-234	-259
TS-4	-171	-213		-180	-196	-210	-206		-182	-245	-243
TS-5		-235	-185	-253	-257	-264	-244	-164	-240	-266	-273
TS-6	-189	-222		-214	-235	-236	-224	-203	-221	-258	-282
TS-7	-184		-190	-218	-227	-225	-220	-199	-234	-259	-250
TS-8G	-258	-246	-253	-256	-285	-286		-253	-236	-234	-224
TS-9G	-237	-244	-251	-248	-245	-248		-227	-223	-234	-209
Mean	-199	-219	-220	-203	-228	-236	-220	-201	-215	-246	-247
St.dev	35	25	37	52	33	27	15	32	39	13	23
Ice complex deposits											
ICD-1	-194	-227	-243	-252	-245	-241	-232	-237	-257	-268	-265
ICD-2			-231	-264	-271	-280	-271	-217	-266	-283	-297
ICD-3				-249	-262	-278	-264	-254	-279	-283	-307
ICD-4			-209	-252	-266	-277	-254	-243	-261	-285	-305
ICD-5			-169	-260	-275	-288	-273	-189	-245	-269	-283
ICD-6	-211	-216	-252	-266	-274	-294	-285	-192	-254	-281	-296
ICD-7			-191	-263	-277	-287	-273	-210	-279	-295	-309
ICD-8	-244	-256	-277	-277	-277	-293	-280	-195	-221	-263	-298
ICD-9	-228	-229	-261	-265	-262	-262	-267	-251	-270	-295	-313
Mean	-219	-232	-229	-261	-268	-278	-267	-221	-259	-280	-297
St.dev	21	17	37	8.6	10	17	16	26	18	12	15

Deleted: KU EXP 1-1, 0-16 cm
Deleted: CH YED2, 0-4 cm
Deleted: SP T3-3B
Deleted: SP T2-7
Deleted: KY T2-3
Deleted: CH T2-1
Deleted: CH YED3, 0-10 cm
Deleted: CH Medv grass
Deleted: CH Y4 grass

Deleted: KU EXP 1-3, 212-216 cm
Deleted: CH YED1, 300-305 cm
Deleted: CH YED2, 300-305 cm
Deleted: CH YED3, 520-525 cm
Deleted: KY EXP1, 0-5 cm
Deleted: KY EXP2, 110-115 cm
Deleted: KY EXP3, 185-200 cm
Deleted: CH DY-3A
Deleted: CH DY-4A

Table 6

Location, sampling depth and isotopic values of samples along a surface sediment transect in the Laptev Sea (data from Bröder et al., 2016b), with percentage topsoil (TS) and ice complex deposit (ICD) OC contributions to the samples based on source-apportionment calculations with $\delta^2\text{H}$ leaf wax end-members versus $\delta^{13}\text{C}-\Delta^{14}\text{C}$ end-members (end-member values are described in the text).

ID ^a	Lat N	Long °E	Depth m	Sample values						Source contributions			
				C ₂₇ ‰	C ₂₉ ‰	C ₃₁ ‰	C ₂₇₋₂₉₋₃₁ ^b ‰	$\delta^{13}\text{C}$ ‰	$\Delta^{14}\text{C}$ ‰	TS using $\delta^2\text{H}$	ICD	TS ^c using $\delta^{13}\text{C}-\Delta^{14}\text{C}$	ICD ^c
TB-46	72.700	130.180	6	-236.2	-237.4	-230.4	-235.0	-26.5	-436	89%	11%	63% (63%)	37% (37%)
YS-9	73.366	129.997	23	-233.7	-231.0	-227.8	-231.1	-26.1	-415	91%	8.9%	63% (65%)	37% (35%)
YS-6	74.724	130.016	32	-234.2	-241.0	-235.4	-236.8	-25.6	-465	86%	14%	51% (59%)	49% (41%)
SW-24	75.599	129.558	46	-229.3	-236.5	-243.5	-236.4	-24.8	-284	87%	13%	70% (72%)	30% (28%)
SW-23	76.171	129.333	56	-219.9	-243.3	-243.3	-236.0	-25.0	-333	83%	17%	65% (70%)	35% (30%)
SW-06	77.142	127.378	92	-219.5	-237.0	-241.4	-233.2	-23.2	-364	87%	13%	39% (53%)	61% (47%)
SW-03	78.238	126.150	2601	-221.1	-238.0	-247.7	-235.9	-22.6	-426	85%	15%	23% (42%)	77% (58%)
SW-01	78.942	125.243	3146	-223.8	-241.8	-246.0	-238.0	-22.3	-418	83%	17%	21% (42%)	79% (58%)

a Location, depth and bulk carbon isotope data from Bröder et al. (2016b)

b weighted average based on individual concentrations

c numbers in brackets are source contributions using the $\delta^{13}\text{C}-\Delta^{14}\text{C}$ approach but with additional corrections for cross-shelf lateral transport time of topsoil OC (similar as in Bröder et al., 2016a); we applied linear aging along the transect based on the distance from the coast, with a maximum aging of 5000 years for station SW-01.

Page 32: [1] Deleted	Jorien			6/7/17 8:36:00 PM		
<i>Mean (median)</i>	5726 (6397)	4310 (4700)	5.9	13	452 (418)	
<i>St.dev (IQR)</i>	3431 (4290)	2190 (4320)	2.7	7.6	230 (332)	

Page 32: [2] Deleted	Jorien			6/7/17 8:36:00 PM		
<i>Mean</i>	22103 (8290)	15160 (6630)	5.0	29	680 (698)	367 (347)
<i>St.dev</i>	35150(5140)	20880 (3510)	1.6	43	163 (176)	85 (81)